



## Epigenetic regulation of TXNIP-mediated oxidative stress and NLRP3 inflammasome activation contributes to SAHH inhibition-aggravated diabetic nephropathy

Xin Dai<sup>a,1</sup>, Ruyi Liao<sup>a,1</sup>, Chaoqun Liu<sup>b,1</sup>, Si Liu<sup>a</sup>, Haiyan Huang<sup>c</sup>, Jianjun Liu<sup>c</sup>, Tianru Jin<sup>d</sup>, Honghui Guo<sup>e</sup>, Zhihua Zheng<sup>a</sup>, Min Xia<sup>f</sup>, Wenhua Ling<sup>f</sup>, Yunjun Xiao<sup>a,\*</sup>

<sup>a</sup> Guangdong Provincial Key Laboratory of Digestive Cancer Research, The Seventh Affiliated Hospital, Sun Yat-sen University, Shenzhen, Guangdong, China

<sup>b</sup> Department of Nutrition, School of Medicine, Jinan University, Guangzhou, Guangdong, China

<sup>c</sup> Key Laboratory of Modern Toxicology of Shenzhen, Shenzhen Center for Disease Control and Prevention, Shenzhen, Guangdong, China

<sup>d</sup> Institute of Medical Science, Department of Physiology, University of Toronto, Toronto, Ontario, Canada

<sup>e</sup> Department of Nutrition, School of Public Health, Guangdong Medical University, Dongguan, Guangdong, China

<sup>f</sup> Guangdong Provincial Key Laboratory of Food, Nutrition and Health, Department of Nutrition, School of Public Health, Sun Yat-sen University, Guangzhou, Guangdong, China

### ARTICLE INFO

#### Keywords:

S-adenosylhomocysteine  
Diabetic nephropathy  
Thioredoxin-interacting protein  
Nod-like receptor protein 3  
Early growth response 1

### ABSTRACT

S-adenosylhomocysteine (SAH) is hydrolyzed by SAH hydrolase (SAHH) to homocysteine and adenosine. Increased plasma SAH levels were associated with disturbed renal function in patients with diabetes. However, the role and mechanism of SAHH in diabetic nephropathy is still unknown. In the present study, we found that inhibition of SAHH by using its inhibitor adenosine dialdehyde (ADA) accumulates intracellular or plasma SAH levels and increases high glucose-induced podocyte injury and aggravates STZ-induced diabetic nephropathy, which is associated with Nod-like receptor protein 3 (NLRP3) inflammasome activation. Inhibition or knockout of NLRP3 attenuates SAHH inhibition-aggravated podocyte injury and diabetic nephropathy. Additionally, SAHH inhibition increases thioredoxin-interacting protein (TXNIP)-mediated oxidative stress and NLRP3 inflammasome activation, but these effects were not observed in TXNIP knockout mice. Mechanistically, SAHH inhibition increased TXNIP by inhibiting histone methyltransferase enhancer of zeste homolog 2 (EZH2) and reduced trimethylation of histone H3 lysine 27 and its enrichment at promoter of early growth response 1 (EGR1). Moreover, EGR1 is activated and enriched at promoters of TXNIP by SAHH inhibition and is essential for SAHH inhibition-induced TXNIP expression. Inhibition of EGR1 protected against SAHH inhibition-induced NLRP3 inflammasome activation and oxidative stress and diabetic nephropathy. Finally, the harmful effects of SAHH inhibition on inflammation and oxidative stress and diabetic nephropathy were also observed in heterozygote SAHH knockout mice. These findings suggest that EZH2/EGR1/TXNIP/NLRP3 signaling cascade contributes to SAHH inhibition-aggravated diabetic nephropathy. Our study firstly provides a novel insight into the role and mechanism of SAHH inhibition in diabetic nephropathy.

### 1. Introduction

Diabetic nephropathy (DN) is the most common chronic microvascular complication of diabetes [1]. It has become a major reason for patients with end stage renal disease (ESRD) [2]. Hyperhomocysteinemia (HHcy) is a risk factor of many different chronic diseases including DN and ESRD [3]. S-adenosylhomocysteine (SAH) is the

metabolic precursor of homocysteine and is reversibly hydrolyzed to homocysteine and adenosine by SAH hydrolase (SAHH). We and other studies showed that SAH is positively associated with cardiovascular risk and is a more sensitive indicator of renal insufficiency than homocysteine [4,5]. Loehrer et al. reported that plasma SAH levels increased by more than 40-fold, whereas plasma tHcy levels only increased by about 5-fold in patients with ESRD [6]. Furthermore, the plasma SAH

\* Corresponding author. The Seventh Affiliated Hospital, Sun Yat-sen University, Shenzhen, Guangdong, China.

E-mail address: [xiaoyj27@mail.sysu.edu.cn](mailto:xiaoyj27@mail.sysu.edu.cn) (Y. Xiao).

<sup>1</sup> The authors contributed equally to the study.

<https://doi.org/10.1016/j.redox.2021.102033>

Received 19 January 2021; Received in revised form 30 May 2021; Accepted 2 June 2021

Available online 5 June 2021

2213-2317/© 2021 The Authors.

Published by Elsevier B.V. This is an open access article under the CC BY-NC-ND license

(<http://creativecommons.org/licenses/by-nc-nd/4.0/>).

levels were also related to disturbed renal function in patients with type 2 diabetes [7]. However, the role and mechanism of increased plasma SAH levels in diabetic nephropathy is still unknown.

The Nod-like receptor protein 3 (NLRP3) inflammasome is a key mediator of innate immune system in response to a host of initiating factors [8–11]. Upon activation, NLRP3 inflammasome transforms the pro-caspase-1 to cleaved caspase-1 and then cleaves the pro-inflammatory cytokines IL-1 $\beta$  to their active forms and induces different cell injury [12]. It has been shown that homocysteine can induce NLRP3 inflammasome activation and podocyte injury [13,14]. However, the effect of SAH on NLRP3 inflammasome activation and podocyte injury independent of homocysteine is still unclear. Thioredoxin-interacting protein (TXNIP) is an upstream partner to NLRP3 and that these two proteins interaction was necessary for NLRP3 inflammasome activation [15,16]. Experimental evidence has shown that hyperglycemia and HHcy can induce TXNIP expression and ROS production [17,18]. SAH has the similar structure of homocysteine and contains a highly reactive thiol group and is readily oxidized to produce ROS [19,20]. However, there is still no direct evidence about the regulation mechanism of SAH on TXNIP expression. And it is still unknown whether TXNIP mediates SAH-induced ROS production.

Epigenetic regulation of TXNIP has been implicated in diabetic kidney disease [21]. SAH is produced as a by-product of methylation of DNA and histone utilizing S-adenosyl-methionine (SAM) as a methyl donor [4,22,23]. The histone methyltransferase enzyme enhancer of zeste homolog 2 (EZH2) is part of the polycomb repressor complex 2, a multi subunit complex, which trimethylates lysine residue 27 on histone 3 (H3K27me3), an epigenetic mark associated with heterochromatin formation and gene silencing [24]. EZH2 depletion increases TXNIP expression and induces oxidative stress and podocyte injury in diabetes [25]. However, it is uncertain whether the effect of EZH2 mediated SAHH inhibition on diabetic nephropathy. In the present study, we used SAHH inhibitor, adenosine dialdehyde (ADA), to investigate the role and mechanism of SAHH inhibition-accumulated SAH in diabetic nephropathy.

## 2. Methods

### 2.1. Experimental animals

The C57BL/6J mice were purchased from The Jackson Laboratory (Bar Harbor, Maine, USA) [23]. NLRP3 knockout (*Nlrp3*<sup>-/-</sup>) mice on a C57BL/6J background were obtained from Jackson Laboratories (Bar Harbor, Maine, USA). TXNIP knockout (*Txnip*<sup>-/-</sup>) mice on a C57BL/6J background were generated by Shanghai Model Organisms Center, Inc. The C57BL/6J mice were randomized to two groups. Diabetes groups were induced by intraperitoneal injections of STZ (40 mg/kg in fresh 0.1 M sodium citrate buffer, pH4.5) daily for 5 days. Control (non-diabetic) groups received citrate buffer. After the last STZ injection, the animals of each group were then further randomized to receive either ADA (1 mg/kg ip twice weekly) or vehicle for 8 weeks. Additionally, *Nlrp3*<sup>-/-</sup> and *Txnip*<sup>-/-</sup> mice and their WT littermate controls at 8 weeks of age were received STZ (40 mg/kg ip injections) daily for 5 days. After the last STZ injection, the mice were further randomized to receive either ADA (1 mg/kg ip twice weekly) or vehicle for 8 weeks. After ADA injections, the mice were individually placed in metabolic cages for 24 h to collect urine samples. To investigate the role of EGR1 in the effect of SAHH inhibition on diabetic nephropathy, the C57BL/6J mice were received STZ daily for 5 days, and then randomized to receive three treatments for 8 weeks, including control, ADA plus scrambled shRNA, and ADA plus EGR1 shRNA (10<sup>9</sup> pfu/mL iv twice weekly). Furthermore, because the homozygous SAHH knockout mice are embryonic lethal, heterozygous SAHH knockout (SAHH<sup>+/-</sup>) mice obtained from Cyagen Biosciences were received STZ daily for 5 days at 8 weeks of age, and then were sacrificed at 8 weeks after STZ injection. The mice were maintained in accordance with standard animal care requirements and

housed in a temperature-controlled (24 °C) room with a 12-h light/dark cycle, with free access to food and autoclaved water. Body weight and food, as well as water intake, were monitored in each group of mice weekly. Blood pressure was measured by tail cuff plethysmography using a noninvasive blood pressure system. The Shenzhen Center for Disease Control and Prevention and Sun Yat-sen University Animal Committees approved all animal experiments.

### 2.2. Cell culture

An immortalized human podocyte cell line was cultured in RPMI-1640 medium supplemented with both 10% fetal bovine serum (FBS) and 100 U/ml penicillin-streptomycin in humidified 5% CO<sub>2</sub> incubator and firstly incubated at 33 °C. After the cells reached at 70% confluence, they were incubated at 37 °C for 2 weeks to allow differentiation before any experimental manipulations. When differentiated cells had grown up to 75% confluence, they were transferred to 2% FBS media for 12 h. These cells were exposed to media containing either normal glucose (as a control, 5.6 mmol/L D-glucose), high glucose (HG, 20 mmol/L D-glucose), ADA (20  $\mu$ mol/L) or SAHH shRNA for 24 h.

### 2.3. Detection of biochemical indexes

At the end of study, mice were anesthetized and exsanguinated by withdrawing the maximum amount of blood from the orbital vein. Fasting blood samples were placed into microtubes containing chilled EDTA and centrifuged immediately at 3000 g for 10 min; plasma was stored at -80 °C until further study. Blood glucose and hemoglobin A<sub>1c</sub> were measured by using a Sysmex XE-2100 Automated hematology analyzer (Roche, Cobas Integra 400). Urine albumin was measured using an ELISA kit (Bethyl Laboratory, Houston, TX), plasma and urine creatinine was measured using a colorimetric assay kit (Abcam). Urinary 8-hydroxy-2'-deoxyguanosine (8-OHdG) was assessed by OxiSelect™ Oxidative DNA damage ELISA kit according to the manufacturer's guidelines (Cell BioLabs). Plasma total homocysteine (tHcy) levels were measured by high-performance liquid chromatography (HPLC) and fluorescence detection [26]. Plasma or intercellular S-adenosylhomocysteine (SAH) and S-adenosylmethionine (SAM) levels were measured by stable-isotope dilution liquid chromatography-electrospray injection tandem mass spectrometry (HPLC-MS/MS) as previously described [27].

### 2.4. SAHH activity assay

The activity of SAHH in kidney tissues was assayed by using a commercial fluorometric kit (Biovision, Mountain View, CA, USA) according to the manufacturer's protocol.

### 2.5. Intracellular ROS measurement

The fluorescent probe DCFH-DA (Beyotime Biotechnology Co., Shanghai, China) was used to measure intracellular ROS. After pretreatment with HG (20 mmol/L), ADA (20  $\mu$ mol/L) in the presence or absence of TXNIP siRNA or scrambled siRNA, AdeZH2 or Ad-control, or anti-miR-101, podocytes were equilibrated for 30 min at 37 °C in Krebs buffer and then incubated with DCFH-DA (10  $\mu$ mol/L) for 20 min at 37 °C in the dark and then examined using a fluorescence microscope (BX51, Olympus).

### 2.6. Western blot analysis

Total protein lysates from the kidney or podocytes were solubilized in SDS-PAGE sample buffer, separated on a 10%–12% SDS-polyacrylamide gel, and transferred electrophoretically onto polyvinylidenedifluoride (PVDF) membranes. Membranes were incubated for 1 h at 24 °C in Tris-buffer saline (TBS)-0.1% Tween-20 containing 5% BSA. Membranes were then incubated overnight at 4 °C with the

primary antibodies to desmin (1:500) (Santa Cruz), synaptopodin (1:500) (Santa Cruz), NLRP3 (1:300) (Abcam), cleaved caspase-1 (1:500) (Cell signaling technology), cleaved gasdermin D (1:500) (Cell signaling technology), TXNIP (1:400) (Abcam), EGR1 (1:500) (Cell signaling technology), EZH2 (1:500) (Cell signaling technology), H3K27me3 (1:500) (Cell signaling technology),  $\beta$ -actin (1:2000) (Abcam), and histone H3 (1:200) (Cell signaling technology). Membranes were then incubated with horseradish peroxidase-conjugated secondary antibodies for 1 h at 24 °C, and developed using a chemiluminescent substrate (Pierce). Band intensities were quantified using Image J software.

## 2.7. Quantitative Real-Time PCR

Total RNA from kidney or podocytes was isolated using TRIzol reagent (Invitrogen) following the manufacturer's instructions. RTqPCR primers for NLRP3, TXNIP, EGR1, and EZH2 were designed using Primer Express software 3.0 and are shown in Table S1. PCR assays were performed using the ABI 7500 machine (Applied Biosystems) and conducted in triplicate wells for each sample. Baseline values of amplification plots were set automatically, and threshold values were kept constant to obtain normalized cycle times and linear regression data. The following reaction mixture per well at a final volume of 20  $\mu$ L was used: 10  $\mu$ L SYBR Green mix I, 0.8  $\mu$ L primers at the final concentration of 10  $\mu$ M, 1  $\mu$ L ROX reference dye, 1  $\mu$ L cDNA, and 7.2  $\mu$ L RNAase free water. For all experiments, the following PCR conditions were used: denaturation at 95 °C for 10 min, followed by 40 cycles at 95 °C for 15 s and then at 60 °C for 60 s. Quantitative normalization of cDNA in each sample was performed using  $\beta$ -actin as internal control. Relative quantification was performed using the  $2^{-\Delta\Delta C_t}$  method.

## 2.8. Immunofluorescent staining of F-actin

To determine whether SAHH inhibition-induced NLRP3 inflammatory activation could result in changes of podocytes cytoskeleton, podocytes were pretreated with caspase-1 inhibitor Z-YVAD (10  $\mu$ mol/L; Biovision, Mountain View, CA, USA) or transfected with NLRP3 siRNA or TXNIP siRNA or scrambled siRNA, and then exposed to HG (20 mmol/L), ADA (20  $\mu$ mol/L) for 48 h. The cells were fixed in 4% paraformaldehyde for 15 min at room temperature after washing, permeabilized for 5 min with 0.1% Triton X-100 in PBS, and blocked for 30 min with 5% BSA. F-actin was stained with phalloidin (Abcam, MA, USA) for 15 min at room temperature. The slides were examined by confocal laser scanning microscopy. The cells with distinct F-actin fibers were counted as described previously [28]. Scoring was obtained from 100 podocytes on each slide in different groups.

## 2.9. Tissue histology and immunohistochemistry or immunofluorescent staining

Kidneys were immediately harvested, fixed in 10% buffered formalin, and embedded in paraffin; 3- $\mu$ m sections were subjected to Periodic Acid Schiff (PAS) and Masson staining. Paraffin-embedded kidney tissue sections were heated at 98 °C for 8 min in citric acid buffer for antigen retrieval, blocked with 0.1% Triton X-100, normal serum of the same species as the secondary antibody, Avidin/Biotin and quenched with 3% hydrogen peroxide. After blocking, sections were incubated with anti- NLRP3 (Abcam) and anti- TXNIP (Abcam) overnight at 4 °C. Biotinylated secondary antibodies were applied and VECTASTAIN® ABC reagents (1: 200, Vector Labs, Burlingame CA) were used according to the manufacturer's instructions. Control sections were incubated with IgG2a isotype antibody (eBioscience). Sections were counterstained with hematoxylin. After staining, randomly choosing glomerular cross sections to calculate positively stained area using Image Pro Plus 6.0 software (Media Cybernetics, Bethesda, MD, USA). The data were exhibited as positively stained area/glomerular area (%).

For SAHH, nephrin, WT-1, F-actin, EZH2, H3K27me3, and EGR1 immunofluorescent staining in kidney tissues or podocytes, sections were incubated with primary antibodies to SAHH (Abcam), nephrin (Abcam), WT-1 (Abcam), F-actin (Abcam), EZH2 (Cell signaling technology), H3K27me3 (Cell signaling technology), and EGR1 (Cell signaling technology) overnight at 4 °C followed by incubation with an Alexa Fluor 594-labeled secondary antibody (1:400, Molecular Probes) and/or Alexa Fluor 488-labeled secondary antibody (1:400, Molecular Probes). The slides were then immersed in ProLong Gold mounting medium with DAPI (Invitrogen) to visualize the nuclei. After staining, randomly choosing glomerular cross sections to calculate positively stained area or cells using Image Pro Plus 6.0 software (Media Cybernetics, Bethesda, MD, USA). The data were exhibited as positively stained area/glomerular area (%) or positively stained cells (%).

## 2.10. Transmission electron microscopy

For detection of ultra structural changes of kidney, tissue samples were fixed with 3% glutaraldehyde in 0.1 mol/L phosphate buffers overnight. Transmission electron microscopy was performed on kidney cortical tissue from four mice of each group. Representative micrographs from each animal were examined using a semiquantitative technique to assess podocyte morphology and identify podocyte abnormalities (adsorption droplets, vacuoles, or pseudocysts) per area glomerulus as previously described [18].

## 2.11. Caspase-1 activity assay

After being transfected with NLRP3 siRNA/scrambled siRNA; TXNIP siRNA/scrambled siRNA, or pretreated with caspase-1 inhibitor (Z-YVAD), podocytes were incubated with HG (20 mmol/L) or ADA (20  $\mu$ mol/L) for 48 h. Caspase-1 activity in supernatant of podocytes and kidney tissues from different groups of mice was assayed by a commercial kit (Biovision, Mountain View, CA, USA), which was used to represent the activation of NLRP3 inflammasome. The data were calculated as the fold changes compared to control cells or mice.

## 2.12. ELISA measurement for IL-1 $\beta$ production

The IL-1 $\beta$  production in supernatant of podocytes and kidney tissues from different groups of mice was measured by ELISA kits according to the protocol described by the manufacturer (R&D Systems, Minneapolis, MN, USA).

## 2.13. Promoter reporter assay

TXNIP promoter-luciferase reporter plasmids (pGL3B-1081) were constructed according to the protocol described previously [23]. Podocytes were seeded in six-well plates 24 h before transfection and transfected with 0.5  $\mu$ g of the TXNIP reporter plasmid, or empty pGL3, along with 0.2  $\mu$ g of a  $\beta$ -galactosidase plasmid (pCMV, Clontech), using jetPEI (Polyplus). Twenty-four hours after transfection, podocytes were incubated with HG (20 mmol/L) or ADA (20  $\mu$ mol/L). Cells were harvested after 24 h, and luciferase and  $\beta$ -galactosidase activities were measured with a reporter assay system (Promega, Madison, MI). Promoter activities are expressed as luciferase values normalized for  $\beta$ -galactosidase.

## 2.14. Chromatin immunoprecipitation (ChIP) assay

ChIP was carried out in kidney tissues or podocytes using the ChIP Assay EZ ChIP kit (Millipore) [29]. Briefly, podocytes or tissues were cross-linked in 1% formaldehyde for 10 min at room temperature. Cross-linking was stopped by addition of glycine to a final concentration of 125 mM for 5 min. Nuclear extracts were prepared by lysing with lysis buffer (50 mM HEPES-KOH pH 7.5, 140 mM NaCl, 1 mM EDTA, 0.1% Triton X-100, 0.1% sodium deoxycholate, with protease inhibitors) and

were resuspended in sonication buffer (0.75%SDS, 2 mM EDTA, and 50 mM Tris-HCl [pH 8.0]). The chromatin was sheared to a final size of 200–500 bp base pairs by sonication with a Bioruptor machine for a total of 20 min with 30-s ‘on’ and 1-min ‘off’ cycles. After preclearing with Protein A or G beads (Upstate), ten percent of original precleared chromatin was removed for use as a control for total input DNA, each ChIP assay was performed using 500 ng of chromatin and 2  $\mu$ L of rabbit polyclonal H3K27me3 and EGR1 primary antibody (Cell Signaling Technology) or normal rabbit IgG (Santa Cruz Biotechnology) incubation overnight at 4 °C with rotation. The next day, Protein A-agarose or Protein G-agarose beads were added and incubated at 4 °C for a further 1–2 h to recover the immune complexes. The complex was washed twice with lysis buffer, once with high salt buffer (50 mM HEPES-KOH pH 7.5, 500 mM NaCl, 1 mM EDTA, 0.1% Triton X-100, 0.1% sodium deoxycholate), twice with LiCl buffer (10 mM Tris-HCl pH 8.0, 0.25 M LiCl, 0.5% Nonidet P40, 0.5% sodium deoxycholate, 1 mM EDTA) and once with TE buffer, followed by elution in TE buffer containing 1% SDS. After washing and elution, DNA was reverse cross-linked overnight at 65 °C, RNase treated for 30 min at 37 °C, proteinase K treated for 2 h at 45 °C, purified using a spin column to a final volume of 50  $\mu$ L, and subjected to analysis by quantitative real-time PCR. PCR was performed with the primer sequences of promoter regions of TXNIP (mouse forward primer, ATATCGGGTGGGCTCTTCT, and reverse, ATTCATGACTCGCCTGAGC; human forward primer, CCTCCTATTCCGTTCCACA, and reverse, TCAGGCCTCATTGTGTGTGT); and EGR1 (mouse forward primer, AGGTGGGATCTCAACCGCA, reverse, TGCA-TACTCGGCCACCAGTC; human forward primer, AACGTGGAGGC-GACGGAAGA, and reverse, CAGTGGCGAGACCCGTTTA) to determine the enrichment of H3K27me3 at promoter region of TXNIP and EGR1, and the enrichment of EGR1 at promoter region of TXNIP. Data were normalized with input control.

### 2.15. ChIP sequencing

ChIP, sequencing library preparation, and data analysis were conducted by LC-Bio (Hangzhou, Zhejiang, China). Genomic DNA degradation and contamination were monitored on 1% agarose gels. DNA purity was checked using the NanoPhotometer® spectrophotometer (IMPLEN, CA, USA). The DNA concentration was measured using a Qubit® DNA Assay Kit in a Qubit® 2.0 Fluorometer (Life Technologies, CA, USA). A total amount of 50 ng DNA per sample was used as input material for the ChIP sample preparations. Sequencing libraries were generated using NEBNext® Ultra™ DNA Library Prep Kit for Illumina® (NEB, USA) following the manufacturer’s recommendations and index codes were added to attribute sequences to each sample. The clustering of the index-coded samples was performed on a cBot Cluster Generation System using a HiSeq Rapid Duo cBot Sample Loading Kit (Illumina) according to the manufacturer’s instructions. After cluster generation, the library preparations were sequenced on an Illumina HiSeq 2500 platform and 50 bp single-end reads were generated. Raw sequencing data were cleaned to filter adapters and low quality reads using FASTQC (v0.11.5) and the unique mapped reads were harvested by mapping the cleaned reads to genome with no more than two mismatches by Bowtie 2. MACS2 (v2.1.1) was used to call peak, giving a robust and high resolution ChIP-Seq peak predictions. Peaks were annotated related genes using Homer (v4.10). DeepTools (v2.4.1) was used to plot gene coverage of the reads near TSS and TES. ChIPseeker (v1.5.1) was used to depict the reads distribution on chromosomes. Homer (v4.10) was used to search motif and analyze transcription factors. The full dataset is available in the National Center for Biotechnology Information Gene Expression Omnibus database with the accession number GSE158210. Raw data are accessible at <https://www.ncbi.nlm.nih.gov/geo/query/acc.cgi?acc=GSE158210>.

### 2.16. Statistical analyses

Results are expressed as means  $\pm$  SEM. Statistical analyses were performed by two-tailed unpaired Student’s *t*-test, Mann-Whitney *U* test, or by one-way or two-way ANOVA followed by Bonferroni posthoc tests to determine statistical significance between the groups. A probability value < 0.05 indicated statistical significance. Statistical analyses were performed using GraphPad Prism software (version 5.0; GraphPad Software Inc., San Diego, CA).

## 3. Results

### 3.1. SAHH inhibition increases high glucose-induced podocyte injury and aggravates STZ-induced diabetic renal injury

To investigate the effect of intracellular SAH accumulation on podocyte, we used the SAHH inhibitor ADA or SAHH shRNA to down-regulate SAHH and accumulate intracellular SAH levels (Fig. S1). SAHH inhibition aggravated high glucose-induced loss of F-actin (Fig. 1A), which is indispensable for the structure and function of podocyte. In addition, SAHH inhibition reduced high glucose-decreased podocyte marker synaptopodin expression. On the contrary, the protein expression of desmin was increased by SAHH inhibition in the presence of high glucose stimulation (Fig. 1B). To explore the effect of SAHH inhibition-accumulated SAH on diabetic renal injury, eight-week aged C57BL/6 mice were intraperitoneally injected with STZ or ADA or their combination. STZ treatment reduced body weight and increased kidney weight, plasma glucose, and hemoglobin A<sub>1c</sub>, but had no significant effect on systolic BP. In contrast, ADA treatment did not change these indicators (Fig. S2). On the other hand, although ADA treatment did not change the protein expression of SAHH, it markedly reduced the activity of SAHH and increased the plasma levels of SAH. However, STZ treatment did not change the protein expression and activity of SAHH and plasma levels of SAH (Fig. 1C and F and Fig. S1). Additionally, ADA treatment aggravated STZ-increased levels of urine albumin and creatinine ratio (UACR) and plasma creatinine (Fig. 1D and E). To evaluate the effects of SAHH inhibition on renal structure, we further examined the pathological changes and glomerular ultra structure of kidneys from different groups. Compared with control, combination of ADA and STZ significantly increased PAS- and Masson-positive area and effacement of the podocyte foot processes and reduced WT-1- and F-actin-positive stained cells compared with control or STZ groups (Fig. 1G–I, Fig. S3A, and Fig. S4A). Taken together, these results suggest that SAHH inhibition aggravated high glucose-induced podocyte injury and STZ-induced diabetic renal injury.

### 3.2. NLRP3 inflammasome activation contributes to SAHH inhibition-aggravated podocyte injury and diabetic nephropathy

To explore the mechanism of SAHH inhibition on renal injury, we further examined the protein expression of NLRP3. Western blot and immunohistochemistry staining showed that the protein expression of NLRP3 was consistently increased by SAHH inhibition in the presence or absence of HG or STZ treatment (Fig. 2A and B). The mRNA levels of NLRP3 were also significantly increased in ADA-treated mice compared with control mice (Fig. 2C). Because the activation of NLRP3 inflammasome transforms the pro-caspase-1 to cleaved caspase-1 and then cleaves IL-1 $\beta$  to its active forms [30]. Hence, we further measured the caspase-1 activity and IL-1 $\beta$  production. We found that SAHH inhibition by ADA noticeably increased IL-1 $\beta$  production and caspase-1 activity in podocyte and kidney homogenates (Fig. 2D). Furthermore, the protein expression of cleaved caspase-1 and gasdermin D were increased by ADA in the presence of HG or STZ treatment in podocyte and kidney homogenates (Fig. S5). To determine whether NLRP3 inflammasome activation mediates SAHH inhibition-induced podocyte injury, we pre-treated podocyte with NLRP3 siRNA or caspase-1 inhibitor Z-YVAD. In

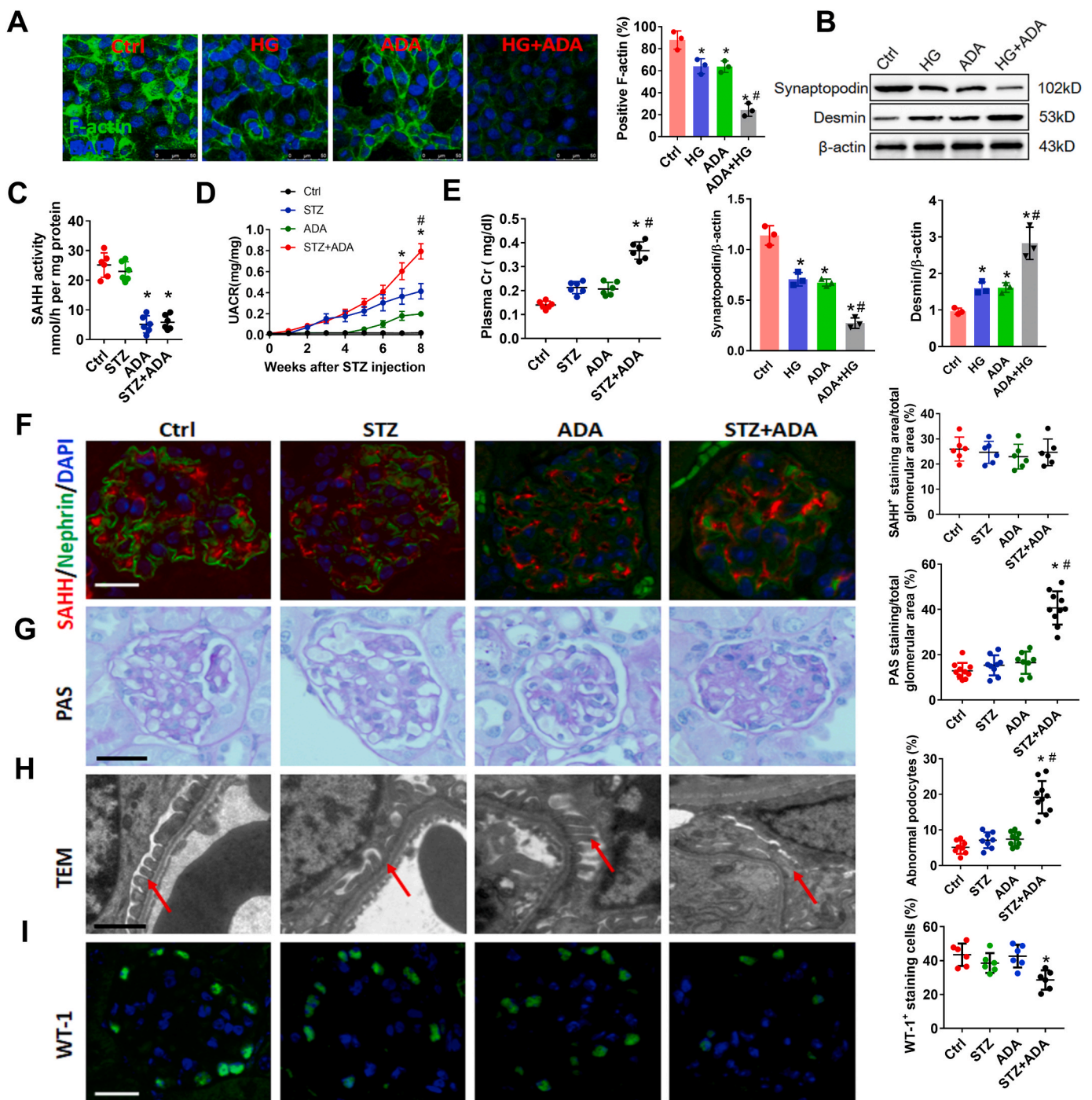


**Fig. 1.** SAHH inhibition increases high glucose-induced podocyte injury and aggravates STZ-induced diabetic nephropathy. (A) Podocytes were incubated with HG (20 mM) or ADA (20  $\mu\text{mol/L}$ ) for 24 h. F-actin was stained with rhodamine-phalloidin and examined by confocal laser scanning microscopy. Scale bar, 50  $\mu\text{m}$ . (B) The protein expression of Desmin and Synaptopodin were assayed by Western blot in podocytes. Values are presented as mean  $\pm$  SEM;  $n = 3$ ,  $*P < 0.05$  vs. control group;  $\#P < 0.05$  vs. HG group (determined by one-way ANOVA). (C) The activity of SAHH in kidney tissues was assayed by using a commercial fluorometric kit. (D–E) Urine albumin was measured using an ELISA kit, plasma and urine creatinine was measured using a colorimetric assay kit. (F) Immunofluorescence staining of SAHH and podocyte marker nephrin in kidney tissues. Scale bar, 20  $\mu\text{m}$ . (G) Glomerular morphological changes were detected using Periodic Acid Schiff (PAS) staining. Scale bar, 20  $\mu\text{m}$ . (H) Representative images and quantitation of podocyte ultrastructure changes by transmission electron microscopy (TEM) examination. Scale bar, 2  $\mu\text{m}$ . (I) Representative immunofluorescence images and quantitation of WT1+ podocytes in glomeruli. Scale bar, 20  $\mu\text{m}$ . Results are mean  $\pm$  SEM;  $n = 6–10$ ,  $*P < 0.05$  vs. Ctrl group;  $\#P < 0.05$  vs. STZ group (determined by one-way ANOVA).

these experiments, either NLRP3 knockdown or caspase-1 inhibition abrogated the SAHH inhibition-induced NLRP3 inflammasome activation and podocyte injury (Fig. 2E–G). To investigate the role of NLRP3 inflammasome activation in SAHH inhibition-induced diabetic nephropathy, we treated *Nlrp3*<sup>-/-</sup> mice with or without ADA. No

significant changes in body weight and plasma glucose of these mice were presented in Fig. S6. NLRP3 knockout abrogated the increased levels of UACR, plasma creatinine, IL-1 $\beta$ , and caspase-1 activity induced by ADA treatment in WT mice (Fig. 3A–C). Furthermore, NLRP3 deficiency protected against SAHH inhibition-induced glomerular

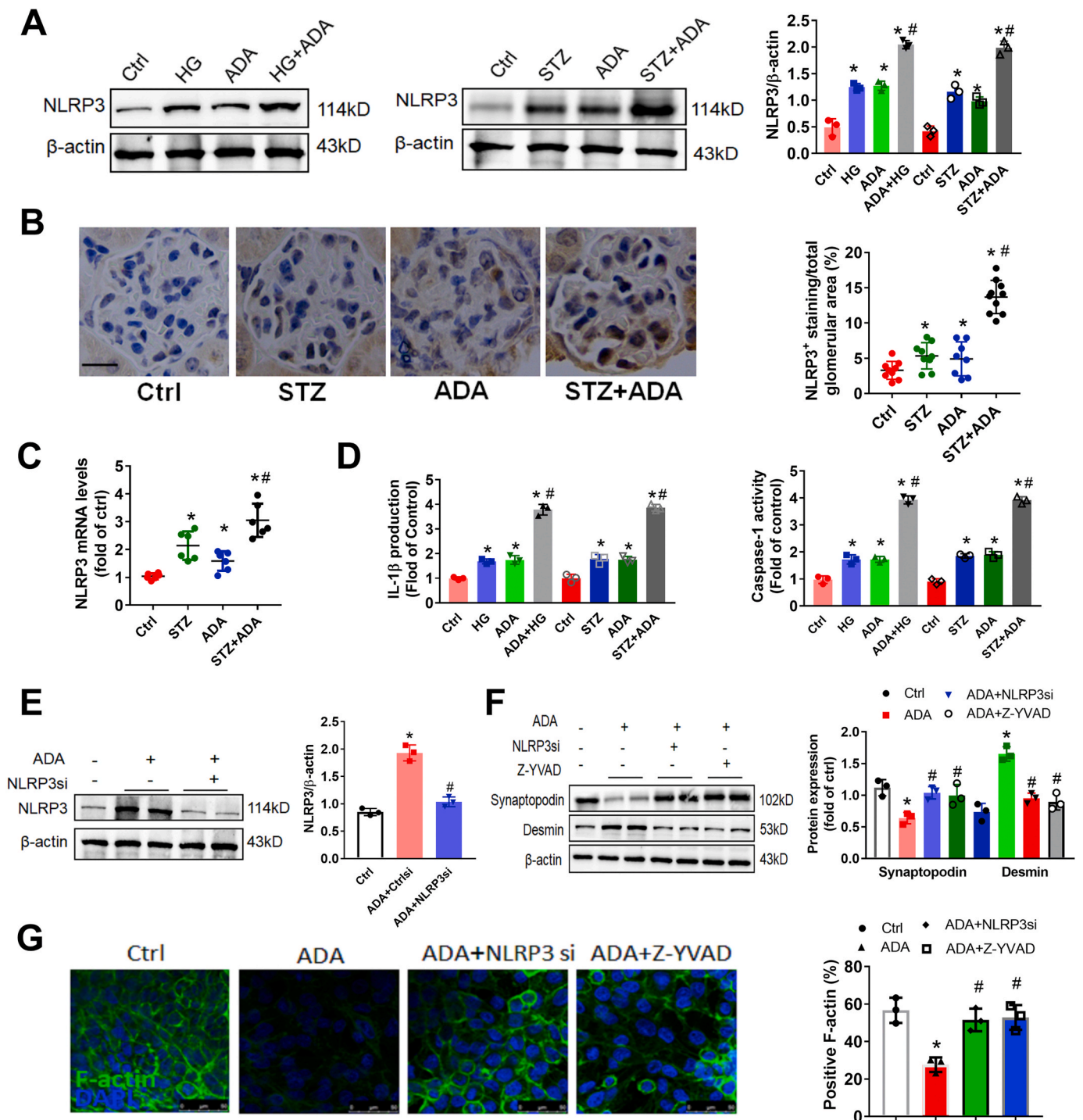


**Fig. 2.** SAHH inhibition increases high glucose-induced NLRP3 inflammasome activation *in vitro* and *in vivo*. (A) The protein expression of NLRP3 was assayed by Western blot in kidney tissues and podocytes. (B) Representative immunohistochemistry staining images and quantitation of NLRP3 expression in kidney tissues sections. Scale bar, 20  $\mu$ m. (C) The mRNA levels of NLRP3 were measured by qRT-PCR *in vivo*. (D) IL-1 $\beta$  production and caspase-1 activity in supernatant of podocytes and kidney tissues was measured by ELISA and commercial kits. (E) The protein expression of NLRP3 was assayed by Western blot in podocytes incubated with ADA (20  $\mu$ mol/L) in the presence or absence of NLRP3 siRNA for 48 h. (F) The protein expression of desmin and synaptopodin were assayed by Western blot in podocytes incubated with ADA (20  $\mu$ mol/L) in the presence or absence of NLRP3 siRNA or caspase-1 inhibitor (Z-YVAD) for 48 h. (G) F-actin was stained with rhodamine-phalloidin and examined by confocal laser scanning microscopy. Scale bar, 50  $\mu$ m. Values are presented as mean  $\pm$  SEM; n = 3, for *in vitro* assays and n = 6–8 for *in vivo* assays, \*P < 0.05 vs. control group; #P < 0.05 vs. ADA or HG (determined by one-way ANOVA or unpaired Student's *t*-test).

extracellular matrix expansion and interstitial fibrosis, loss of podocyte and F-actin, and effacement of podocyte foot processes (Fig. 3D–F, Fig. S3B, and Fig. S4B). Taken together, our observations suggest that NLRP3 inflammasome activation contributes to SAHH inhibition-aggravated podocyte injury and diabetic nephropathy.

### 3.3. SAHH inhibition induced TXNIP expression and increased oxidative stress *in vivo* and *in vitro*

Because thioredoxin-interacting protein (TXNIP) as a binding partner to NLRP3, the association between these two proteins was necessary

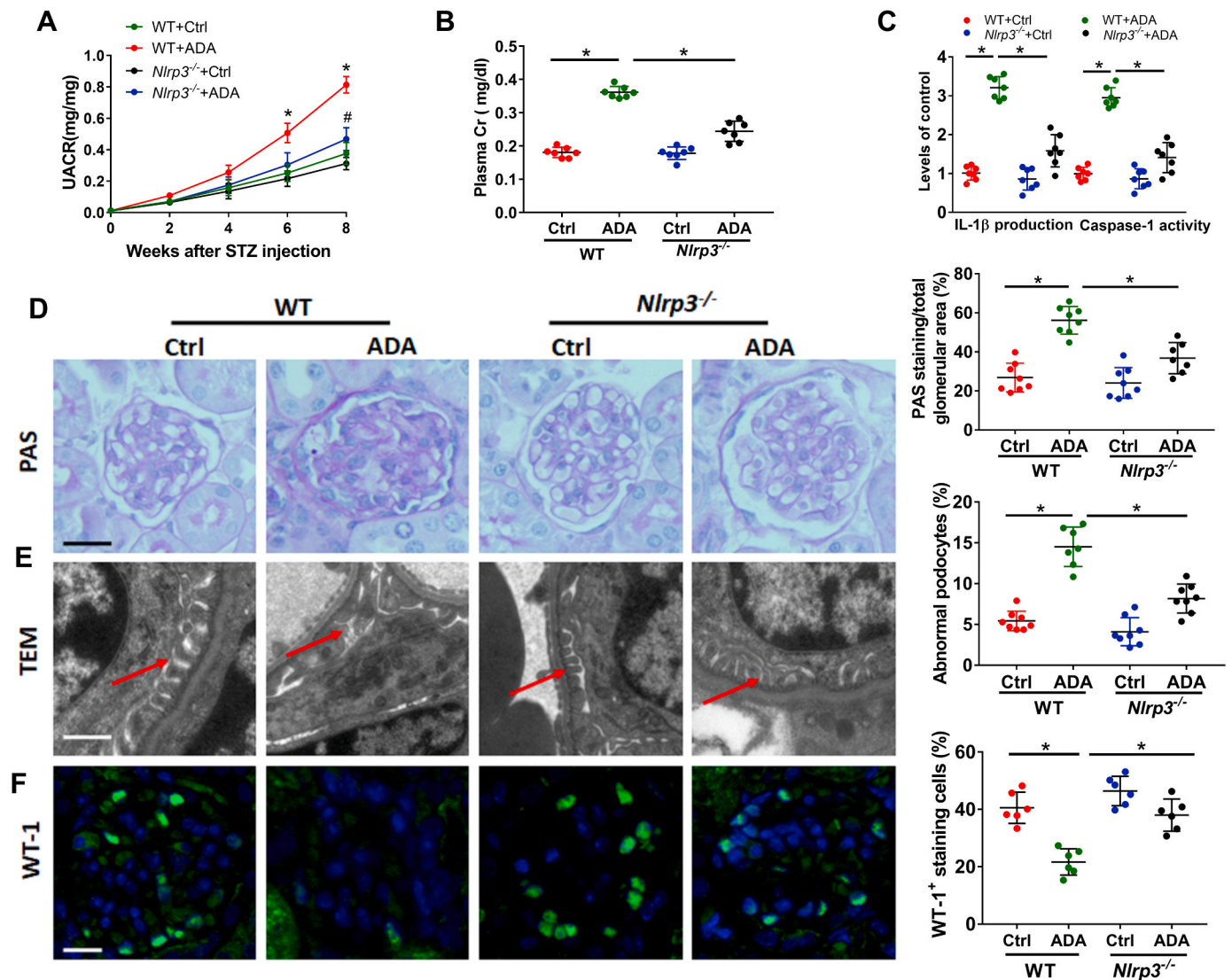


**Fig. 3.** Knockout of NLRP3 attenuates SAHH inhibition-aggravated diabetic nephropathy. (A–B) Urine albumin and creatinine were measured using commercial kits. (C) IL-1 $\beta$  production and caspase-1 activity in kidney tissues was measured by commercial kits. (D) Glomerular morphological changes and quantitation were detected using PAS staining. Scale bar, 20  $\mu$ m. (E) Representative podocyte ultrastructure changes and quantitation of podocyte abnormalities (%) by TEM examination. Scale bar, 2  $\mu$ m. (F) Representative immunofluorescence images and quantitation of WT-1<sup>+</sup> podocytes in glomeruli. Scale bar, 20  $\mu$ m. Results are mean  $\pm$  SEM; n = 6–8, \* $P$  < 0.05 vs. ADA-treated WT mice (determined by one-way ANOVA).

for downstream inflammasome activation. Therefore, we further focused on TXNIP, the negative regulator of the antioxidant TRX, dissociate from TRX to bind with NLRP3 [15]. ADA treatment increased protein expression of TXNIP in podocytes in the presence or absence of high glucose. Furthermore, the mRNA and protein expression of TXNIP was dramatically increased in kidney tissues of ADA-treated mice injected with STZ compared to control mice (Fig. 4A–C). Because TXNIP contributes to redox status of cells and can promote cell oxidative injury [16], we further tested the effect of SAHH inhibition on the levels of ROS in podocytes. As shown in Fig. 4D, combination of ADA with high glucose significantly augmented ROS production to levels greater than ADA or high glucose treatment alone. Additionally, the urinary levels of oxidative stress marker 8-hydroxy-2'-deoxyguanosine (8-OHdG) were significantly increased in ADA-treated mice compared to control mice with or without STZ injection (Fig. 4E).

#### 3.4. Downregulation of TXNIP alleviates SAHH inhibition-induced NLRP3 inflammasome activation and diabetic nephropathy

To evaluate whether TXNIP mediates SAHH inhibition-induced NLRP3 inflammasome activation, podocyte was transfected with TXNIP siRNA or scrambled siRNA. As expected, TXNIP siRNA transfection attenuated SAHH inhibition-increased ROS generation (Fig. 4F–G). Furthermore, downregulation of TXNIP abolished SAHH inhibition-induced NLRP3 inflammasome activation, including decreased protein expression of NLRP3, IL-1 $\beta$  production and caspase-1 activity (Fig. 4H–I). Additionally, these findings were further verified in *Txnip*<sup>-/-</sup> mice. The changes of body weight and glucose were showed in Fig. S7. In agree with *in vitro* findings, TXNIP knockout decreased the urinary levels of 8-OHdG in *Txnip*<sup>-/-</sup> mice compared to ADA-treated WT mice (Fig. 5A). Moreover, the NLRP3 inflammasome activation was blocked in *Txnip*<sup>-/-</sup> mice compared to their littermate WT mice with ADA treatment (Fig. 5B and D). *Txnip*<sup>-/-</sup> mice had a significant reduction in UACR and plasma creatinine compared with WT mice treated with ADA (Fig. 5C). TXNIP deficiency attenuated the PAS- and Masson-

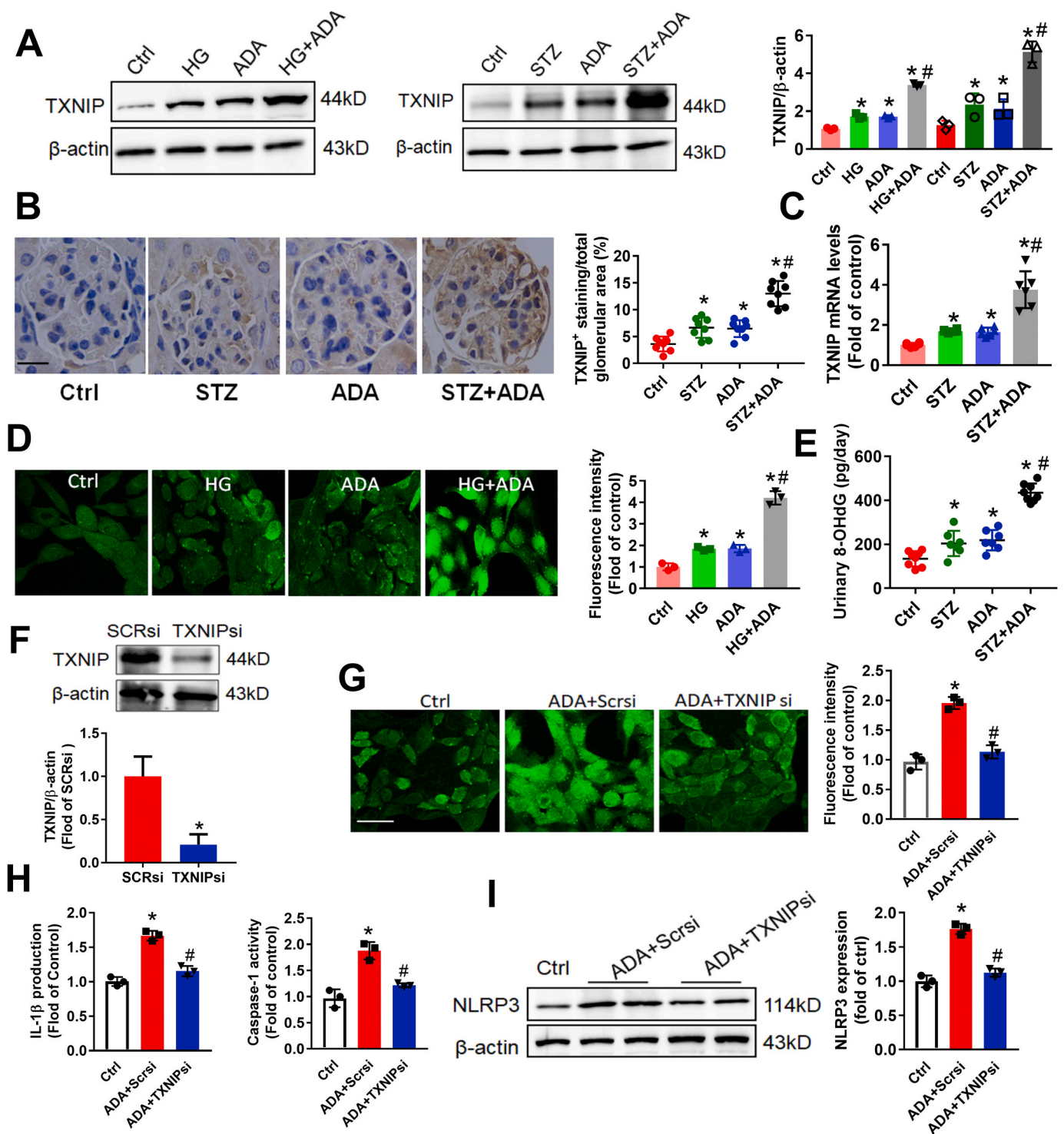


**Fig. 4.** SAHH inhibition induced TXNIP expression and increased oxidative stress *in vivo* and *in vitro*. (A) Protein expression of TXNIP was assayed by Western blot *in vivo* and *in vitro*. (B) Immunohistochemistry staining and quantitation analyses of TXNIP expression in kidney tissues. Scale bar, 20  $\mu$ m. (C) The mRNA levels of TXNIP were measured by quantitative RT-PCR. (D) Intracellular ROS production was measured by DCF staining and examined using a fluorescence microscope. Scale bar, 50  $\mu$ m. (E) Urinary levels of oxidative stress marker 8-hydroxy-2'-deoxyguanosine (8-OHdG) were measured by an ELISA kit according to the manufacturer's protocol. (F) Protein expression of TXNIP was assayed by Western blot in podocytes incubated with TXNIP siRNA transfection. (G) Intracellular ROS production was measured by DCF staining and examined using a fluorescence microscope. Scale bar, 50  $\mu$ m. (H) Caspase-1 activity and IL-1 $\beta$  production in supernatant was measured by commercial kits. (I) The protein expression of NLRP3 was assayed by Western blot in podocytes. Values are mean  $\pm$  SEM;  $n = 3$  for *in vitro* assays and  $n = 6-8$  for *in vivo* assays, \* $P < 0.05$  vs. control group; # $P < 0.05$  vs. ADA group (determined by one-way ANOVA).

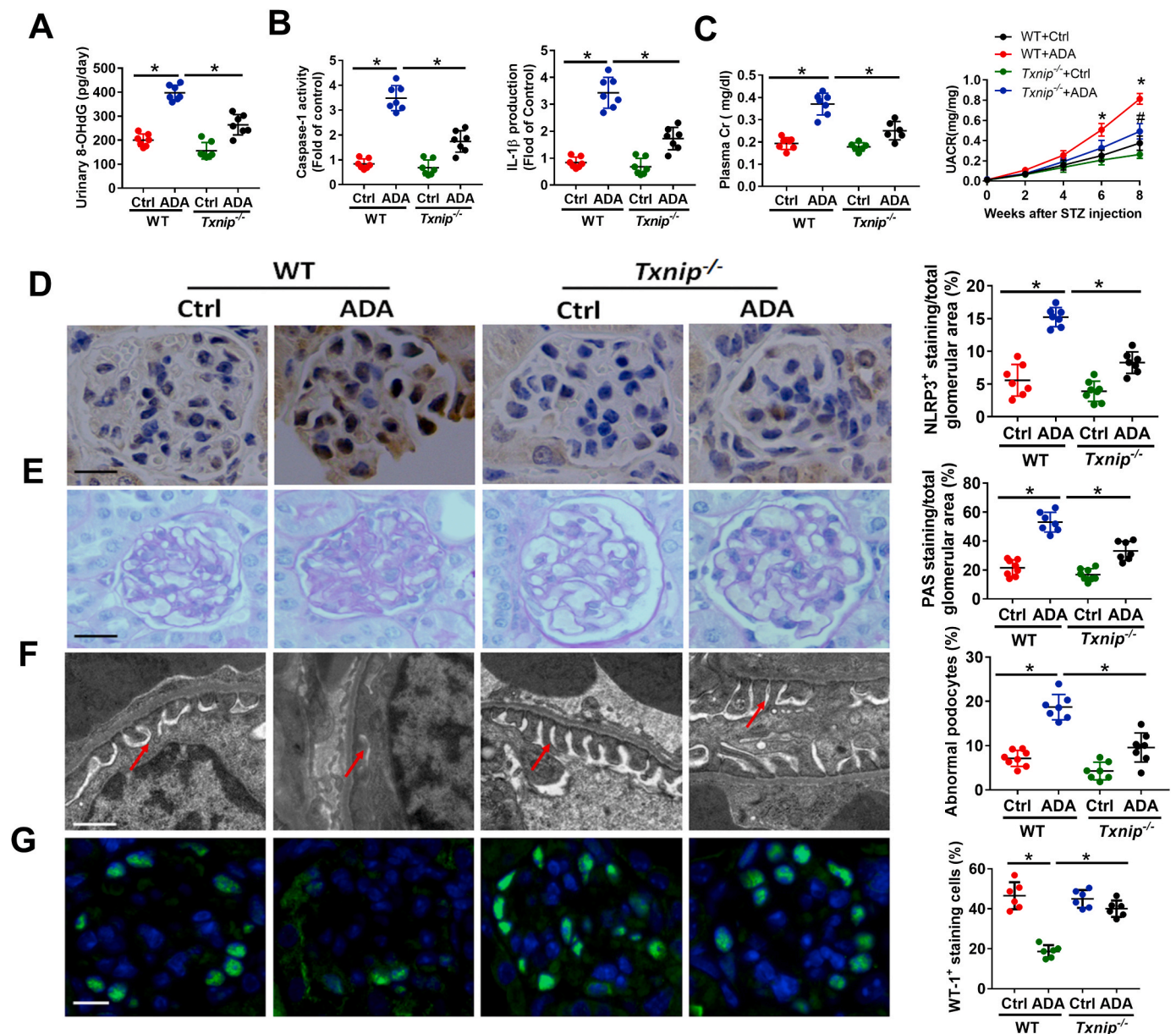


**Fig. 5.** TXNIP mediated SAHH inhibition-induced NLRP3 inflammasome activation and diabetic nephropathy. (A) Urinary levels of 8-OHdG were measured by an ELISA kit. (B) Caspase-1 activity and IL-1 $\beta$  production in kidney tissues was measured by commercial kits. (C) Urine albumin and creatinine was measured using commercial kits. (D) Immunohistochemistry staining and quantitation analyses of NLRP3 in kidney tissues. Scale bar, 20  $\mu$ m. (E) Glomerular morphological changes were detected using PAS staining. Scale bar, 20  $\mu$ m. (F) Representative podocyte ultrastructure changes and quantitation of podocyte abnormalities (%) by TEM examination. Scale bar, 2  $\mu$ m. (G) Representative immunofluorescence images and quantitation of WT1+ podocytes in glomeruli. Scale bar, 20  $\mu$ m. Values are mean  $\pm$  SEM; n = 6–8 for *in vivo* assays, \* $P$  < 0.05 vs. ADA-injected WT mice (determined by one-way ANOVA or unpaired Student's *t*-test).

positive area and numbers of abnormal podocyte and increased WT-1- and F-actin-positive staining in *Txnip*<sup>-/-</sup> mice compared to their littermate WT mice treated with ADA (Fig. 5E–G, Fig. S3C, and Fig. S4C). Collectively, our findings suggest that TXNIP-mediated NLRP3 inflammasome activation is essential for SAHH inhibition-aggravated diabetic nephropathy.

### 3.5. SAHH inhibition increased TXNIP by inhibiting EZH2 expression

It has been reported that EZH2 can negatively regulates TXNIP expression, oxidative stress, and podocyte injury [25]. To examine how SAHH inhibition regulates TXNIP, we next sought to explore whether SAHH inhibition increased TXNIP expression by inhibiting EZH2. Western blot and immunofluorescent staining showed that the protein

expression of EZH2 was markedly decreased in ADA-treated mice in the presence of STZ pretreatment (Fig. 6A and B). In agree with *in vivo* results, SAHH inhibition by ADA treatment dramatically reduced the protein expression of EZH2 in podocyte in the presence of high glucose condition. EZH2 is mainly responsible for trimethylation of H3K27 (H3K27me3), which was also decreased by ADA treatment in the presence or absence of high glucose stimulation (Fig. 6C). Consistently, knockdown of EZH2 by siRNA reduced expression of H3K27me3 and increased TXNIP and ROS production (Fig. S8). Conversely, we next asked the question as to whether upregulation of EZH2 would attenuate these processes induced by SAHH inhibition. Thus, we infected podocytes with adenovirus plasmids expressing EZH2 (AdeZH2) or control. AdeZH2 infection increased protein expression of EZH2 and H3K27me3, attenuated the protein expression of TXNIP and ROS generation induced

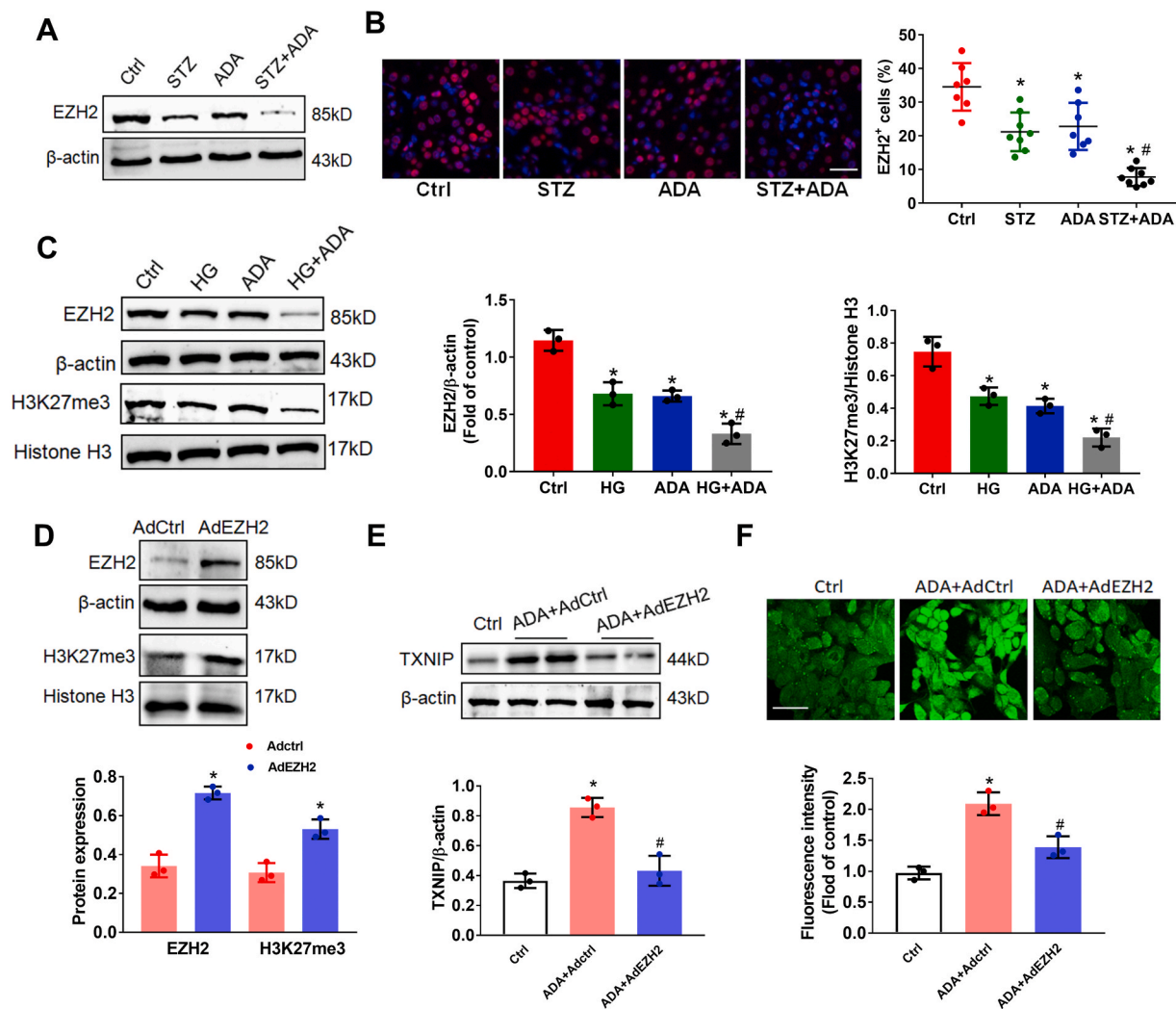


**Fig. 6.** SAHH inhibition increased TXNIP by inhibiting EZH2 expression. (A) Protein expression of EZH2 was assayed by Western blot in kidney tissues. (B) Representative immunofluorescence images and quantitation of EZH2 expression in kidney tissues sections. Scale bar, 20  $\mu\text{m}$ . (C) Protein expression of EZH2 and H3K27me3 were assayed by Western blot in podocytes. (D) Protein expression of EZH2 and H3K27me3 were assayed by Western blot in podocytes treated with AdEZH2 or AdCtrl. (E) Protein expression of TXNIP was assayed by Western blot in podocytes treated with ADA (20  $\mu\text{mol/L}$ ) with or without AdEZH2 infection. (F) Intracellular ROS production was measured by DCF staining in podocytes treated with ADA (20  $\mu\text{mol/L}$ ) with or without AdEZH2 infection. Values are mean  $\pm$  SEM;  $n = 3$  for *in vitro*, 6–8 for *in vivo* assays, \* $P < 0.05$  vs. control or Adctrl group; # $P < 0.05$  vs. ADA group (determined by one-way ANOVA or unpaired Student's *t*-test).

by SAHH inhibition (Fig. 6D–F). Additionally, it has been established that miR-101 can negatively regulate EZH2 expression [24,31,32]. To test whether miR-101 inhibition would augment EZH2 expression and abolish the SAHH inhibition-induced TXNIP expression and ROS generation, we used a sequence-specific oligonucleotide inhibitor (anti-miR-101) to antagonize its effects in podocytes. In agree with previous studies, treatment with anti-miR-101 resulted in a strikingly increased protein expression of EZH2 and H3K27me3. Similarly, anti-miR-101 treatment abrogated the SAHH inhibition-induced TXNIP protein expression and ROS generation (Fig. S9).

### 3.6. The transcription factor EGR1 is required for SAHH inhibition-induced TXNIP expression

Next, to investigate whether SAHH inhibition induced TXNIP expression by reducing the enrichment of histone repressive marker H3K27me3 at the promoter of TXNIP, we employed chromatin immunoprecipitation (ChIP) to determine the enrichment of H3K27me3 at TXNIP promoters. Unexpectedly, we found that the enrichment of H3K27me3 at TXNIP promoters was not significantly changed by ADA treatment in podocyte (Fig. 7A). These results enable us to post a

question whether EZH2 regulated TXNIP expression through the repression of H3K27me3 at the promoter of other *trans*-acting factors. We performed ChIP sequencing and compared the differential peaks between ADA and control and found that the enrichment of H3K27me3 at promoter of early growth response 1 (EGR1) was the maximum significant decreased peak in ADA group compared with control (Fig. 7B). We further verified that the protein expression of EGR1 was significantly increased by ADA treatment in podocyte (Fig. 7C). Moreover, to localize the protein expression of EGR1, immunofluorescent staining showed that the protein expression of EGR1 is colocalized in nucleus with H3K27me3 and is simultaneously increased by ADA treatment with or without high glucose (Fig. 7D). Similarly results of the EGR1 and H3K27me3 protein expression were observed *in vivo* (Fig. 7E). To test whether EGR1 directly binds with the promoter of TXNIP and regulates its expression, we performed ChIP and binding sites prediction by JASPAR database and verified by luciferase activity assay. We found that SAHH inhibition increased the enrichment of EGR1 at the promoter of TXNIP in podocyte (Fig. 7F). Overexpression of EGR1 increased promoter activity of TXNIP in full-length promoter cloned plasmid. By deleting different fragments of promoter of TXNIP, we found that the fragment from 335 to 727 is required for EGR1-increased promoter

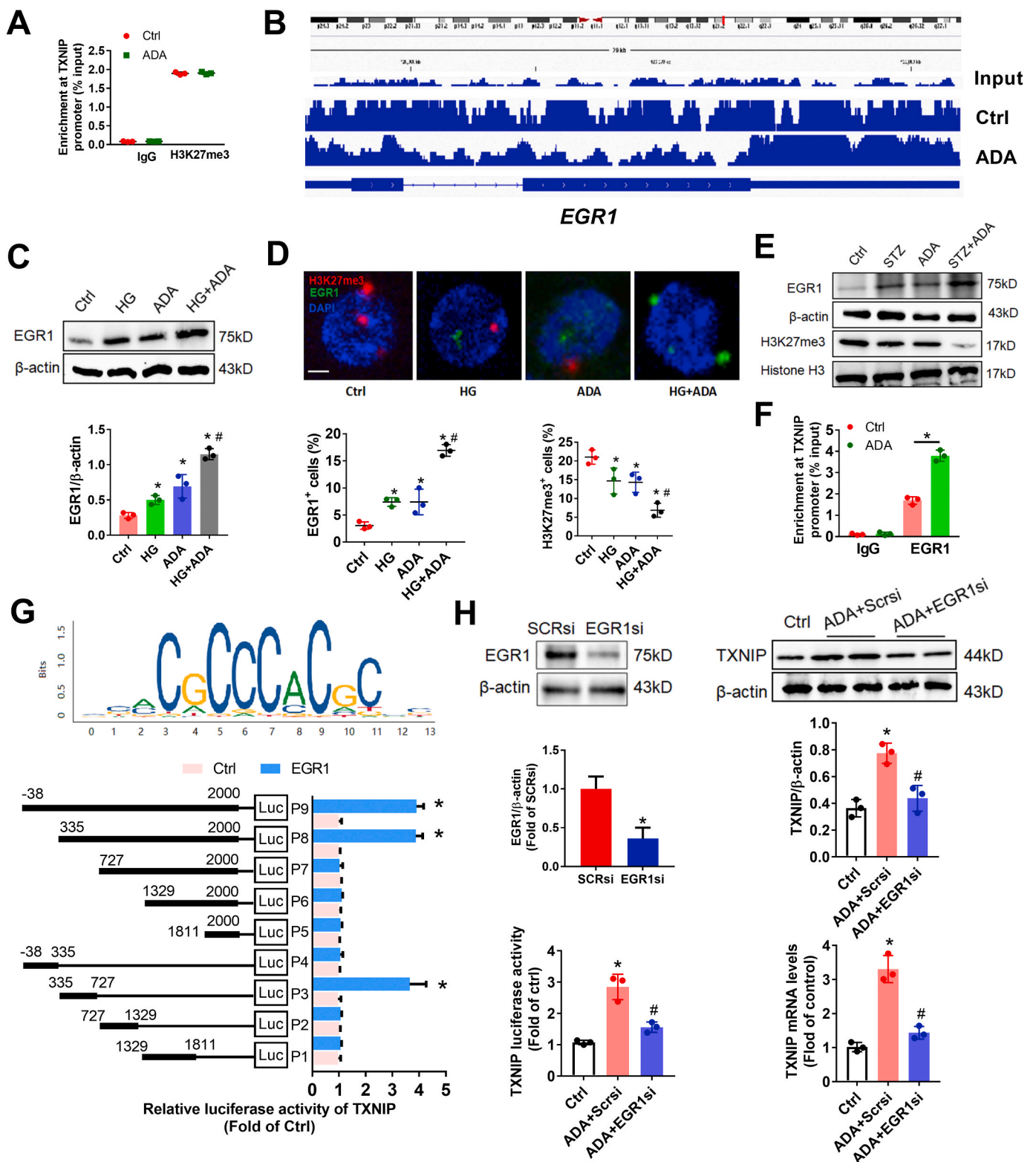


**Fig. 7. Transcription factor EGR1 is required for SAHH inhibition-induced TXNIP expression.** (A) Podocytes were incubated with ADA (20  $\mu$ mol/L) for 24 h. The enrichment of H3K27me3 at TXNIP promoter in podocytes was assayed by chromatin immunoprecipitation (ChIP). (B) ChIP sequencing showed the enrichment of H3K27me3 at EGR1 promoter were decreased in ADA-treated mice compared with control. (C) Protein expression of EGR1 was assayed by Western blot in podocytes. (D) Representative immunofluorescence images and quantitation of H3K27me3 and EGR1 expression in podocytes. Scale bar, 2  $\mu$ m. (E) The protein expression of H3K27me3 and EGR1 were assayed by Western blot in kidney tissues. (F) The enrichment of EGR1 at TXNIP promoter was assayed by ChIP in podocytes. (G) The motif of EGR1 from JASPAR database was used to predict the binding sites on TXNIP promoter. The luciferase activity of TXNIP promoter was measured by a reporter assay system. (H) The protein and mRNA expression of TXNIP and its promoter activity were measured in podocytes treated by ADA with or without EGR1 siRNA transfection. Values are mean  $\pm$  SEM; n = 3 for *in vitro*, 6–8 for *in vivo* assays, \* $P$  < 0.05 vs. control; # $P$  < 0.05 vs. ADA (determined by one-way ANOVA or unpaired Student's *t*-test).

activity of TXNIP (Fig. 7G), suggesting that this fragment is the potential position where EGR1 directly binds at the promoter of TXNIP. Additionally, we examine whether the expression of EGR1 is necessary for SAHH inhibition-induced TXNIP expression. Downregulation of EGR1 by transfecting with EGR1 siRNA significantly abolished SAHH inhibition-increased the protein and mRNA expression and promoter activity of TXNIP (Fig. 7H). Collectively, these results suggest that EGR1 is a critical transcription factor for SAHH inhibition-increased TXNIP expression.

### 3.7. Knockdown of EGR1 alleviates SAHH inhibition-increased inflammation and diabetic nephropathy

To investigate whether inhibition of EGR1 could protect against SAHH inhibition-induced inflammation and diabetic nephropathy, we intraperitoneally injected C57BL/6 mice with ADA in the presence or absence of tail vein injection of EGR1 shRNA for 8 weeks. As shown in Fig. 8A, EGR1 shRNA treatment did not change the body or kidney weight, blood glucose, and blood pressure. However, compared with scrambled shRNA, EGR1 shRNA treatment significantly reduced the kidney injury, such as less mesangial hyperplasia, glycogen deposition, and interstitial fibrosis, and more numbers of podocyte foot processes, WT-1 and F-actin positive staining (Fig. 8B). Moreover, downregulation

of EGR1 abolished SAHH inhibition-induced NLRP3 inflammasome activation, oxidative stress, and renal function injury (Fig. 8C-E). Western blot showed that the protein expression of TXNIP and NLRP3 were significantly decreased by EGR1 shRNA treatment (Fig. 8F). These findings suggest that activation of EGR1 may mediate the harmful effect of SAHH inhibition on diabetic nephropathy.

### 3.8. Knockdown of SAHH increases oxidative stress and inflammation and diabetic nephropathy

Finally, we investigate the role of SAHH in diabetic nephropathy in SAHH knockout mice and SAHH shRNA-transfected podocyte. The basic characteristics were not significant different between SAHH<sup>-/-</sup> and wild type mice at 8 weeks after STZ injection. Plasma SAH levels were increased whereas SAM/SAH ratios were decreased in SAHH<sup>-/-</sup> mice compared with wild type mice (Fig. 9A). The protein levels of SAHH were obviously reduced in SAHH<sup>-/-</sup> mice (Fig. 9B). More PAS- and Masson-positive staining and numbers of abnormal podocyte and less WT-1- and F-actin-positive staining were observed in SAHH<sup>-/-</sup> mice compared with wild type mice (Fig. 9C). Furthermore, knockout of SAHH increased renal function injury and levels of inflammation and oxidative stress (Fig. 9D). SAHH shRNA transfection decreased F-actin expression and increased ROS levels in podocyte (Fig. 9E). Consistently,

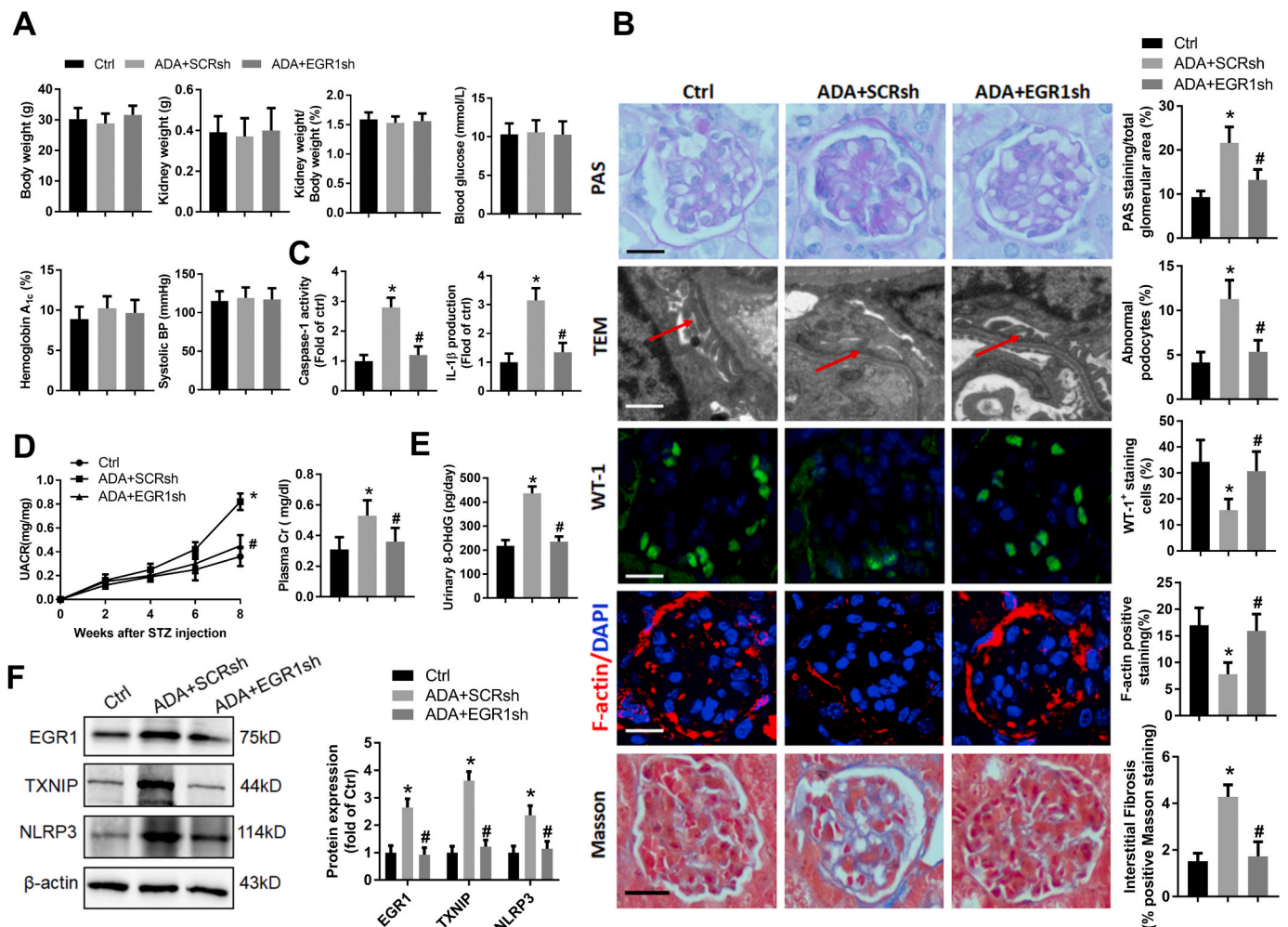


**Fig. 8. Knockdown of EGR1 alleviates SAHH inhibition-increased inflammation and diabetic nephropathy.** (A) The basic characteristics of C57BL/6 mice injected with ADA in the presence or absence of tail vein injection of EGR1 shRNA, (B) Representative images and quantitation of PAS staining, TEM examination, WT1, F-actin, and Masson staining, (C) The levels of caspase-1 activity and IL-1 $\beta$  production in kidney tissues were measured by commercial kits. (D) Urine albumin and creatinine was measured using commercial kits. (E) Urinary levels of 8-OHdG were measured by an ELISA kit. (F) Protein expression of EGR1, TXNIP, and NLRP3 was assayed by Western blot. Values are mean  $\pm$  SEM; n = 6–8, \*P < 0.05 vs. control; #P < 0.05 vs. scrambled shRNA (determined by one-way ANOVA).

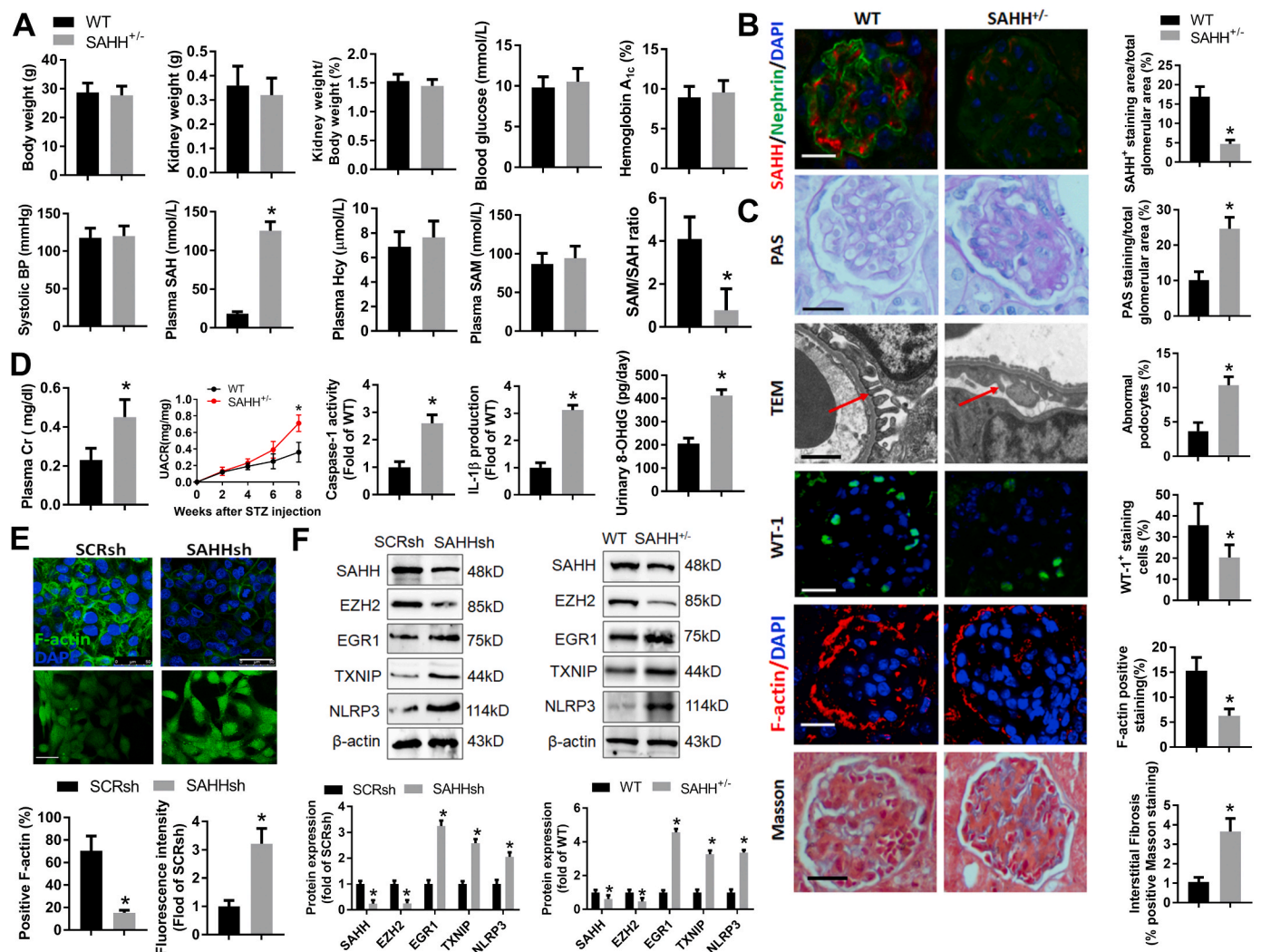


**Fig. 9.** Knockdown of SAHH increases oxidative stress and inflammation and diabetic nephropathy. (A) The basic characteristics and plasma methionine metabolites levels of SAHH<sup>+/-</sup> and wild type mice, (B–C) Representative images and quantitation of SAHH immunofluorescence staining, PAS staining, TEM examination, WT1, F-actin, and Masson staining, (D) The levels of caspase-1 activity and IL-1β production, urine albumin and creatinine, and urinary levels of 8-OHdG was measured by commercial kits. (E) Representative images and quantitation of F-actin staining and ROS levels in podocytes treated with SAHH shRNA. (F) Protein expression of SAHH, EZH2, EGR1, TXNIP, and NLRP3 was assayed by Western blot *in vitro* and *in vivo*. Values are mean ± SEM; n = 3 for *in vitro*, 6–8 for *in vivo* assays, \*P < 0.05 vs. WT (determined by unpaired Student's *t*-test).

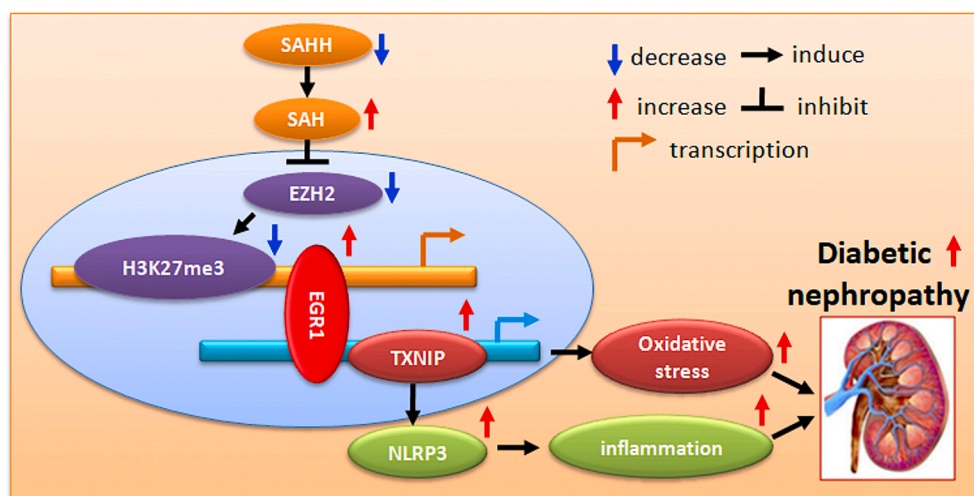


**Fig. 10.** Schematic shows that SAHH inhibition aggravates diabetic nephropathy via epigenetic regulation of TXNIP-mediated NLRP3 inflammasome activation.

downregulation of SAHH decreased the expression of EZH2 and increased the expression of EGR1, TXNIP and NLRP3 *in vitro* and *in vivo* (Fig. 9F). Taken together, these results suggest that knockdown of SAHH resulted in SAH accumulation may aggravate diabetic renal injury through inhibition of EZH2-mediated activation of EGR1-TXNIP-NLRP3 pathway.

#### 4. Discussion

In the present study, we firstly demonstrate that SAHH inhibition resulted in SAH accumulation and promote high glucose-induced podocyte injury and aggravated diabetic nephropathy. Mechanistically, SAHH inhibition decreased EZH2 expression and thereby reduced H3K27me3 expression and its enrichment at promoter of EGR1. Interestingly, SAHH inhibition increased EGR1 expression and its binding to promoters of TXNIP and then induced TXNIP-mediated oxidative stress and NLRP3 inflammasome activation, and ultimately accelerated diabetic nephropathy (Fig. 10). Our study provides important insight on the effect and mechanism of SAHH inhibition on high SAH-related diabetic nephropathy.

It has previously been shown that rat podocytes express the intermediate filaments desmin. In healthy control rats, desmin is mainly located within mesangial cells and vascular smooth muscle cells with very weak staining in podocytes. Increased desmin expression is a sensitive marker of very early podocyte injury. WT-1 is strongly expressed in podocytes throughout ontogeny serving as a specific marker. It is also present in the nuclei of differentiated podocytes in the adult kidneys, suggesting a key role for WT-1 in the maintenance of podocyte function. Recent studies of patients and diabetic animal models reported downregulation of both synaptopodin and WT-1 in diabetic nephropathy, and it was concluded that this downregulation may be either related to a phenotypic podocyte change or podocyte loss [33]. Renal dysfunction is a critical complication of diabetes [1]. Plasma levels of tHcy and SAH were increased and positively associated with degree of renal injury in diabetic nephropathy [7]. However, neither tHcy nor SAH correlated to the markers of diabetes such as hemoglobin A<sub>1c</sub>, an indicator of long-term diabetes control, suggesting that probably advanced renal injury, but not diabetes itself, is associated with disturbed Hcy metabolism [7]. Consistent with this suggestion, although we used STZ to induce diabetic nephropathy and found that the levels of blood glucose and hemoglobin A<sub>1c</sub> were significantly increased in STZ-treated mice, ADA treatment did not change the levels of blood glucose and hemoglobin A<sub>1c</sub>. These findings suggest that although SAHH inhibition increased plasma SAH levels, this did not change the status of diabetes. Hence, the SAHH inhibition-aggravated diabetic nephropathy may be independent of blood glucose changes. Furthermore, a bulk of studies has reported a high incidence of HHcy in renal patients. These studies have also suggested that SAH mediated the harmful effects of Hcy in the vascular system [4,34,35], for example, SAH but not Hcy was associated with renal vascular vasodilatory dysfunction [36]. Additionally, plasma SAH is also a more sensitive indicator of renal insufficiency and much stronger associated with the degree of impaired renal function than plasma Hcy [5,7]. In the present study, we found that SAHH inhibition resulted in increased plasma SAH levels with normal plasma Hcy levels, indicating that the injury of SAHH inhibition on diabetic nephropathy might be partially attributed to plasma SAH levels independently of plasma Hcy levels.

The activation of NLRP3 inflammasomes has been implicated in a growing number of diverse pathogenesis of various diseases [10,11,37]. Numbers of initiate factors can activate NLRP3 inflammasomes including high glucose and HHcy [13,14,30]. Consistent with these studies, we found SAHH inhibition by ADA can also activate and further accelerate high glucose-induced NLRP3 inflammasomes activation. These findings suggest SAHH inhibition-accumulated high SAH may produce similar pro-inflammatory effect of HHcy in the normal Hcy conditions [15,38–40]. Importantly, it has been confirmed that TXNIP

binding to NLRP3 is essential for ROS-mediated NLRP3 inflammasomes activation in the pathogenesis of diabetic nephropathy [30]. In resting cells, TXNIP interacts with thioredoxin (TRX) and thereby blocks the anti-oxidative ability of TRX and is unavailable for NLRP3 inflammasome activation. After an increase in ROS caused by stimulation such as glucose, Hcy, or SAH, TXNIP is released from oxidized TRX and in turn binds NLRP3 and induces NLRP3 inflammasome activation. When knockdown of TXNIP results in an increased anti-oxidative ability of TRX and reduced ROS levels, and therefore decreases the expression of NLRP3 and its activation-induced IL-1 $\beta$  production [15].

Additionally, TXNIP can be up-regulated by high glucose, fructose, and Hcy [13,41,42]. SAH has a highly reactive thiol group similar to the structure of Hcy and can be easily oxidized to produce ROS [43]. We and other studies have shown that increased SAH can increase ROS production by different mechanisms in various conditions [19,23,44,45]. However, whether TXNIP participates in SAH-induced ROS production in diabetic nephropathy is unknown. Therefore, in the present study, we assess whether SAHH inhibition resulted in SAH accumulation and then induced TXNIP-mediated ROS production and NLRP3 inflammasomes activation. As expected, SAHH inhibition increased the expression of TXNIP and the levels of ROS. Moreover, knockout of TXNIP protect against SAHH inhibition-induced diabetic nephropathy, which is in agreement with the findings that protective role of TXNIP deficiency in diabetic nephropathy [18]. Taken together, these finding suggest that TXNIP-mediated NLRP3 inflammasomes activation is essential for SAHH inhibition-induced diabetic nephropathy.

Epigenetic regulation of gene expression plays important role in varieties of diseases and is mediated by posttranslational modifications of the chromatin structure, including acetylation and methylation of the histone tails [46]. It has been demonstrated that hyperglycemia-induced TXNIP expression was associated with stimulation of activating histone marks acetylation of H3K9 and decrease in the repressor histone mark H3K27me3 at the promoter region of TXNIP [21]. EZH2 is the main methyltransferase enzyme for methylating H3K27me3. It has been reported that EZH2 depletion decreased H3K27me3 expression, whereas increases TXNIP expression and induces oxidative stress and renal injury in diabetes [25]. Among the posttranslational modifications, SAH as a product of methylation negatively feedback regulates methylation status by competitively inhibiting methyltransferase enzyme [47,48]. However, whether SAHH inhibition-induced TXNIP expression was associated with SAH-inhibited EZH2 and H3K27me3 expression is unknown. In the present study, we found that SAHH inhibition by ADA significantly reduced EZH2 and H3K27me3 expression. Overexpression of EZH2 by adenovirus abolished SAHH inhibition-induced TXNIP expression and podocyte injury. Agreement with the effect of miR-101 in inhibiting EZH2 translation [24,31,32], inhibition of miR-101 increased EZH2 and H3K27me3 expression and produced similar effect. These results indicate that inhibition of EZH2 due to accumulation of SAH maybe explain the SAHH inhibition-induced TXNIP expression and podocyte injury.

Next, to test whether SAHH inhibition-induced TXNIP expression is attributed to decrease in the enrichment of repressor histone mark H3K27me3 at the promoter region of TXNIP, we performed ChIP and ChIP sequencing. Interestingly, we found that SAHH inhibition did not change the enrichment of H3K27me3 at TXNIP promoter, which is inconsistent with previous study that hyperglycemia-induced TXNIP was associated with decreased enrichment of H3K27me3 at TXNIP promoter in human mesangial cells [21]. On the other hand, the binding of H3K27me3 to TXNIP promoter was undetectable in DZNep-treated podocytes [25]. These discrepancies may be explained by the different experimental conditions such as different cells or treatments. These results enable us to pose a question whether there may be other *trans*-acting factors mediated the repression of EZH2 on TXNIP expression. Bioinformatics analyses of ChIP sequencing data showed that ADA treatment decreased the enrichment of H3K27me3 at EGR1 promoter. Additionally, SAHH inhibition increased EGR1 expression and its

enrichment at the promoter of TXNIP and thereby increased the luciferase activity of TXNIP promoter. EGR1 knockdown abolished the SAHH inhibition-induced TXNIP expression, suggesting that EGR1 is essential for SAHH inhibition-induced transcription activation of TXNIP. It has been demonstrated that EGR1 plays important roles in diabetic kidney disease involving in the regulation of oxidative stress [49], inflammation [50,51], and fibrosis process [51,52]. Podocytes EGR1 were increased in proteinuric patients and mice, whereas loss of EGR1 in mice protects from renal inflammation and fibrosis and reduced proteinuria and glomerulosclerosis [52–54]. Taken together, our findings suggest that SAHH inhibition might regulate TXNIP expression in an EGR1-dependent manner by inhibiting EZH2-methylated H3K27me3 expression.

In conclusion, our study provided direct evidence that SAHH inhibition induced high SAH-related diabetic nephropathy via EZH2-EGR1-TXNIP-NLRP3 signaling cascade. These findings elucidate a novel molecular mechanism for explanation the association between high plasma SAH levels and renal dysfunction and uncover new potential therapeutic targets for the treatment and prevention of end stage renal disease with high SAH.

## Funding

This work was supported by grants from the National Natural Science Foundation of China (82073530, 81730090, 81402672), and Guangdong Provincial Medical Research Fund (A2019017), Shenzhen Science and Technology Plan Project (JCYJ20190809144001733), and China Postdoctoral Fund (2017M612624), and Guangdong Provincial Key Laboratory of Digestive Cancer Research (No. 2021B1212040006).

## Declaration of competing interest

None declared.

## Appendix A. Supplementary data

Supplementary data to this article can be found online at <https://doi.org/10.1016/j.redox.2021.102033>.

## References

- [1] S. Dronavalli, I. Duka, G.L. Bakris, The pathogenesis of diabetic nephropathy, *Nat. Clin. Pract. Endocrinol. Metabol.* 4 (2008) 444–452.
- [2] J.L. Gross, M.J. de Azevedo, S.P. Silveiro, L.H. Canani, M.L. Caramori, T. Zelmanovitz, Diabetic nephropathy: diagnosis, prevention, and treatment, *Diabetes Care* 28 (2005) 164–176.
- [3] W. Herrmann, M. Herrmann, R. Obeid, Hyperhomocysteinaemia: a critical review of old and new aspects, *Curr. Drug Metabol.* 8 (2007) 17–31.
- [4] Y. Xiao, Y. Zhang, M. Wang, X. Li, D. Su, J. Qiu, D. Li, Y. Yang, M. Xia, W. Ling, Plasma S-adenosylhomocysteine is associated with the risk of cardiovascular events in patients undergoing coronary angiography: a cohort study, *Am. J. Clin. Nutr.* 98 (2013) 1162–1169.
- [5] C. Wagner, W.J. Stone, M.J. Koury, W.D. Dupont, D.M. Kerins, S-adenosylhomocysteine is a more sensitive indicator of renal insufficiency than homocysteine, *Nutr. Res.* 24 (2004) 487–494.
- [6] F.M. Loehrer, C.P. Angst, F.P. Brunner, W.E. Haefeli, B. Fowler, Evidence for disturbed S-adenosylmethionine : S-adenosylhomocysteine ratio in patients with end-stage renal failure: a cause for disturbed methylation reactions? *Nephrol. Dial. Transplant.* 13 (1998) 656–661.
- [7] W. Herrmann, H. Schorr, R. Obeid, J. Makowski, B. Fowler, M.K. Kuhlmann, Disturbed homocysteine and methionine cycle intermediates S-adenosylhomocysteine and S-adenosylmethionine are related to degree of renal insufficiency in type 2 diabetes, *Clin. Chem.* 51 (2005) 891–897.
- [8] P. Duewell, H. Kono, K.J. Rayner, C.M. Sirois, G. Vladimer, F.G. Bauernfeind, G. S. Abela, L. Franchi, G. Nunez, M. Schnurr, T. Espevik, E. Lien, K.A. Fitzgerald, K. L. Rock, K.J. Moore, S.D. Wright, V. Hornung, E. Latz, NLRP3 inflammasomes are required for atherogenesis and activated by cholesterol crystals, *Nature* 464 (2010) 1357–1361.
- [9] R.C. Coll, A.A. Robertson, J.J. Chae, S.C. Higgins, R. Munoz-Planillo, M.C. Inerra, I. Vetter, L.S. Dungan, B.G. Monks, A. Stutz, D.E. Croker, M.S. Butler, M. Haneklaus, C.E. Sutton, G. Nunez, E. Latz, D.L. Kastner, K.H. Mills, S.L. Masters, K. Schroder, M.A. Cooper, L.A. O'Neill, A small-molecule inhibitor of the NLRP3 inflammasome for the treatment of inflammatory diseases, *Nat. Med.* 21 (2015) 248–255.
- [10] A. Abderrazak, D. Couchie, D.F. Mahmood, R. Elhage, C. Vindis, M. Laffargue, V. Mateo, B. Buchele, M.R. Ayala, M. El Gaafary, T. Syrovets, M.N. Slimane, B. Friguet, T. Fulop, T. Simmet, K. El Hadri, M. Rouis, Anti-inflammatory and antiatherogenic effects of the NLRP3 inflammasome inhibitor arglabin in ApoE2.Ki mice fed a high-fat diet, *Circulation* 131 (2015) 1061–1070.
- [11] W. Zhu, F.S. Cao, J. Feng, H.W. Chen, J.R. Wan, Q. Lu, J. Wang, NLRP3 inflammasome activation contributes to long-term behavioral alterations in mice injected with lipopolysaccharide, *Neuroscience* 343 (2017) 77–84.
- [12] H. Shi, Y. Wang, X. Li, X. Zhan, M. Tang, M. Fina, L. Su, D. Pratt, C.H. Bu, S. Hildebrand, S. Lyon, L. Scott, J. Quan, Q. Sun, J. Russell, S. Arnett, P. Jurek, D. Chen, V.V. Kravchenko, J.C. Mathison, E.M. Moresco, N.L. Mornson, R. J. Ulevitch, B. Beutler, NLRP3 activation and mitosis are mutually exclusive events coordinated by NEK7, a new inflammasome component, *Nat. Immunol.* 17 (2016) 250–258.
- [13] J.M. Abais, M. Xia, G. Li, Y. Chen, S.M. Conley, T.W. Gehr, K.M. Boini, P.L. Li, Nod-like receptor protein 3 (NLRP3) inflammasome activation and podocyte injury via thioredoxin-interacting protein (TXNIP) during hyperhomocysteinemia, *J. Biol. Chem.* 289 (2014) 27159–27168.
- [14] C. Zhang, K.M. Boini, M. Xia, J.M. Abais, X. Li, Q. Liu, P.L. Li, Activation of Nod-like receptor protein 3 inflammasomes turns on podocyte injury and glomerular sclerosis in hyperhomocysteinemia, *Hypertension* 60 (2012) 154–162.
- [15] R. Zhou, A. Tardivel, B. Thorens, I. Choi, J. Tschopp, Thioredoxin-interacting protein links oxidative stress to inflammasome activation, *Nat. Immunol.* 11 (2010) 136–140.
- [16] J. Chen, G. Saxena, I.N. Mungro, A.J. Lusa, A. Shalev, Thioredoxin-interacting protein: a critical link between glucose toxicity and beta-cell apoptosis, *Diabetes* 57 (2008) 938–944.
- [17] T.B. Koenen, R. Stienstra, L.J. van Tits, J. de Graaf, A.F. Stalenhoef, L.A. Joosten, C. J. Tack, M.G. Netea, Hyperglycemia activates caspase-1 and TXNIP-mediated IL-1beta transcription in human adipose tissue, *Diabetes* 60 (2011) 517–524.
- [18] A. Shah, L. Xia, E.A. Masson, C. Gui, A. Momen, E.A. Shikata, M. Husain, S. Quaggin, R. John, I.G. Fantus, Thioredoxin-interacting protein deficiency protects against diabetic nephropathy, *J. Am. Soc. Nephrol.* 26 (2015) 2963–2977.
- [19] J.A. Sipkens, N.E. Hahn, H.J. Blom, S.M. Loughheed, C.D. Stehouwer, J. A. Rauwerda, P.A. Krijnen, V.W. van Hinsbergh, H.W. Niessen, S-Adenosylhomocysteine induces apoptosis and phosphatidylserine exposure in endothelial cells independent of homocysteine, *Atherosclerosis* 221 (2012) 48–54.
- [20] A. Araki, Y. Sako, Y. Fukushima, M. Matsumoto, T. Asada, T. Kita, Plasma sulfhydryl-containing amino acids in patients with cerebral infarction and in hypertensive subjects, *Atherosclerosis* 79 (1989) 139–146.
- [21] Y. De Marinis, M. Cai, P. Bompada, D. Atac, O. Kotova, M.E. Johansson, E. Garcia-Vaz, M.F. Gomez, M. Laakso, L. Groop, Epigenetic regulation of the thioredoxin-interacting protein (TXNIP) gene by hyperglycemia in kidney, *Kidney Int.* 89 (2016) 342–353.
- [22] Y. Xiao, W. Huang, J. Zhang, C. Peng, M. Xia, W. Ling, Increased plasma S-Adenosylhomocysteine-Accelerated atherosclerosis is associated with epigenetic regulation of endoplasmic reticulum stress in apoE<sup>-/-</sup> mice, *Arterioscler. Thromb. Vasc. Biol.* 35 (2015) 60–70.
- [23] Y. Xiao, J. Xia, J. Cheng, H. Huang, Y. Zhou, X. Yang, X. Su, Y. Ke, W. Ling, Inhibition of S-adenosylhomocysteine hydrolase induces endothelial dysfunction via epigenetic regulation of p66shc-mediated oxidative stress pathway, *Circulation* 139 (2019) 2260–2277.
- [24] S. Varambally, Q. Cao, R.S. Mani, S. Shankar, X. Wang, B. Ateeq, B. Laxman, X. Cao, X. Jing, K. Ramnarayanan, J.C. Brenner, J. Yu, J.H. Kim, B. Han, P. Tan, C. Kumar-Sinha, R.J. Lonigro, N. Palanisamy, C.A. Maher, A.M. Chinnaiyan, Genomic loss of microRNA-101 leads to overexpression of histone methyltransferase EZH2 in cancer, *Science* 322 (2008) 1695–1699.
- [25] F.S. Siddiqui, S. Majumder, K. Thai, M. Abdalla, P. Hu, S.L. Advani, K.E. White, B. B. Bowskill, G. Guarna, C.C. Dos Santos, K.A. Connelly, A. Advani, The histone methyltransferase enzyme enhancer of zeste homolog 2 protects against podocyte oxidative stress and renal injury in diabetes, *J. Am. Soc. Nephrol.* 27 (2016) 2021–2034.
- [26] J.B. Ubbink, W.J. Hayward Vermaak, S. Bissbort, Rapid high-performance liquid chromatographic assay for total homocysteine levels in human serum, *J. Chromatogr.* 565 (1991) 441–446.
- [27] H. Gellekink, D. van Oppenraaij-Emmerzaal, A. van Rooij, E.A. Struys, M. den Heijer, H.J. Blom, Stable-isotope dilution liquid chromatography-electrospray injection tandem mass spectrometry method for fast, selective measurement of S-adenosylmethionine and S-adenosylhomocysteine in plasma, *Clin. Chem.* 51 (2005) 1487–1492.
- [28] F.F. He, C. Zhang, S. Chen, B.Q. Deng, H. Wang, N. Shao, X.J. Tian, Z. Fang, X. F. Sun, J.S. Liu, Z.H. Zhu, X.F. Meng, Role of CD2-associated protein in albumin overload-induced apoptosis in podocytes, *Cell Biol. Int.* 35 (2011) 827–834.
- [29] R. Patel, M. Patel, R. Tsai, V. Lin, A.L. Bookout, Y. Zhang, L. Magomedova, T. Li, J. F. Chan, C. Budd, D.J. Mangelsdorf, C.L. Cummins, LXRBeta is required for glucocorticoid-induced hyperglycemia and hepatosteatosis in mice, *J. Clin. Invest.* 121 (2011) 431–441.
- [30] P. Gao, X.F. Meng, H. Su, F.F. He, S. Chen, H. Tang, X.J. Tian, D. Fan, Y.M. Wang, J. S. Liu, Z.H. Zhu, C. Zhang, Thioredoxin-interacting protein mediates NALP3 inflammasome activation in podocytes during diabetic nephropathy, *Biochim. Biophys. Acta* 1843 (2014) 2448–2460.
- [31] I. Floris, B. Descamps, A. Vardeu, T. Mitic, A.M. Posadino, S. Shantikumar, G. Sala-Newby, G. Capobianco, G. Mangialardi, L. Howard, S. Dessole, R. Urrutia, G. Pintus, C. Emanuelli, Gestational diabetes mellitus impairs fetal endothelial cell

- functions through a mechanism involving microRNA-101 and histone methyltransferase enhancer of zester homolog-2, *Arterioscler. Thromb. Vasc. Biol.* 35 (2015) 664–674.
- [32] N.M. Alajez, W. Shi, A.B. Hui, J. Bruce, M. Lenarduzzi, E. Ito, S. Yue, B. O'Sullivan, F.F. Liu, Enhancer of Zeste homolog 2 (EZH2) is overexpressed in recurrent nasopharyngeal carcinoma and is regulated by miR-26a, miR-101, and miR-98, *Cell Death Dis.* 1 (2010) e85.
- [33] J. Funk, V. Ott, A. Herrmann, W. Rapp, S. Raab, W. Riboulet, A. Vandjour, E. Hainaut, A. Benardeau, T. Singer, B. Jacobsen, Semiautomated quantitative image analysis of glomerular immunohistochemistry markers desmin, vimentin, podocin, synaptopodin and WT-1 in acute and chronic rat kidney disease models, *Histochem. Cell Biol.* 145 (2016) 315–326.
- [34] A. Valli, J.J. Carrero, A.R. Qureshi, G. Garibotto, P. Barany, J. Axelsson, B. Lindholm, P. Stenvinkel, B. Anderstam, M.E. Suliman, Elevated serum levels of S-adenosylhomocysteine, but not homocysteine, are associated with cardiovascular disease in stage 5 chronic kidney disease patients, *Clin. Chim. Acta* 395 (2008) 106–110.
- [35] D.M. Kerins, M.J. Koury, A. Capdevila, S. Rana, C. Wagner, Plasma S-adenosylhomocysteine is a more sensitive indicator of cardiovascular disease than plasma homocysteine, *Am. J. Clin. Nutr.* 74 (2001) 723–729.
- [36] A.S. De Vriese, H.J. Blom, S.G. Heil, S. Mortier, L.A. Kluijtmans, J. Van de Voorde, N.H. Lameire, Endothelium-derived hyperpolarizing factor-mediated renal vasodilatory response is impaired during acute and chronic hyperhomocysteinemia, *Circulation* 109 (2004) 2331–2336.
- [37] Y.D. Xiao, Y.Y. Huang, H.X. Wang, Y. Wu, Y. Leng, M. Liu, Q. Sun, Z.Y. Xia, Thioredoxin-interacting protein mediates NLRP3 inflammasome activation involved in the susceptibility to ischemic acute kidney injury in diabetes, *Oxid. Med. Cell Longev.* (2016) 2386068, 2016.
- [38] A. Babelova, K. Moreth, W. Tsalastra-Greul, J. Zeng-Brouwers, O. Eickelberg, M. F. Young, P. Bruckner, J. Pfeilschifter, R.M. Schaefer, H.J. Grone, L. Schaefer, Biglycan, a danger signal that activates the NLRP3 inflammasome via toll-like and P2X receptors, *J. Biol. Chem.* 284 (2009) 24035–24048.
- [39] L.K. Jones, K.M. O'Sullivan, T. Semple, M.P. Kuligowski, K. Fukami, F.Y. Ma, D. J. Nikolic-Paterson, S.R. Holdsworth, A.R. Kitching, IL-1RI deficiency ameliorates early experimental renal interstitial fibrosis, *Nephrol. Dial. Transplant.* 24 (2009) 3024–3032.
- [40] A. Vilaysane, J. Chun, M.E. Seamone, W. Wang, R. Chin, S. Hirota, Y. Li, S.A. Clark, J. Tschopp, K. Trpkov, B.R. Hemmelgarn, P.L. Beck, D.A. Muruve, The NLRP3 inflammasome promotes renal inflammation and contributes to CKD, *J. Am. Soc. Nephrol.* 21 (2010) 1732–1744.
- [41] W. Qi, X. Chen, R.E. Gilbert, Y. Zhang, M. Waltham, M. Schache, D.J. Kelly, C. A. Pollock, High glucose-induced thioredoxin-interacting protein in renal proximal tubule cells is independent of transforming growth factor-beta1, *Am. J. Pathol.* 171 (2007) 744–754.
- [42] X. Zhang, J.H. Zhang, X.Y. Chen, Q.H. Hu, M.X. Wang, R. Jin, Q.Y. Zhang, W. Wang, R. Wang, L.L. Kang, J.S. Li, M. Li, Y. Pan, J.J. Huang, L.D. Kong, Reactive oxygen species-induced TXNIP drives fructose-mediated hepatic inflammation and lipid accumulation through NLRP3 inflammasome activation, *Antioxidants Redox Signal.* 22 (2015) 848–870.
- [43] M.H. Stipanuk, Sulfur amino acid metabolism: pathways for production and removal of homocysteine and cysteine, *Annu. Rev. Nutr.* 24 (2004) 539–577.
- [44] X. Luo, Y. Xiao, F. Song, Y. Yang, M. Xia, W. Ling, Increased plasma S-adenosylhomocysteine levels induce the proliferation and migration of VSMCs through an oxidative stress-ERK1/2 pathway in apoE(-/-) mice, *Cardiovasc. Res.* 95 (2012) 241–250.
- [45] M. Barroso, C. Florindo, H. Kalwa, Z. Silva, A.A. Turanov, B.A. Carlson, I.T. de Almeida, H.J. Blom, V.N. Gladyshev, D.L. Hatfield, T. Michel, R. Castro, J. Loscalzo, D.E. Handy, Inhibition of cellular methyltransferases promotes endothelial cell activation by suppressing glutathione peroxidase 1 protein expression, *J. Biol. Chem.* 289 (2014) 15350–15362.
- [46] B.E. Bernstein, A. Meissner, E.S. Lander, The mammalian epigenome, *Cell* 128 (2007) 669–681.
- [47] S.J. James, S. Melnyk, M. Pogribna, I.P. Pogribny, M.A. Caudill, Elevation in S-adenosylhomocysteine and DNA hypomethylation: potential epigenetic mechanism for homocysteine-related pathology, *J. Nutr.* 132 (2002) 2361S–2366S.
- [48] O. Saavedra, L. Isakovic, D. Llewellyn, L. Zhan, N. Bernstein, S. Claridge, F. Raepel, A. Vaisburg, N. Elowe, A. Petschner, J. Rahil, N. Beaulieu, A. MacLeod, D. Delorme, J. Besterman, A. Wahhab, SAR around (1)-S-adenosylhomocysteine, an inhibitor of human DNA methyltransferase (DNMT) enzymes, *Bioorg. Med. Chem. Lett* 19 (2009) 2747–2751.
- [49] F. Hu, M. Xue, Y. Li, Y.J. Jia, Z.J. Zheng, Y.L. Yang, M.P. Guan, L. Sun, Y.M. Xue, Early growth response 1 (Egr1) is a transcriptional activator of NOX4 in oxidative stress of diabetic kidney disease, *J. Diabetes Res.* (2018) 3405695, 2018.
- [50] C. Wu, X. Ma, Y. Zhou, Y. Liu, Y. Shao, Q. Wang, Klotho restraining egr1/TLR4/mTOR Axis to reducing the expression of fibrosis and inflammatory cytokines in high glucose cultured rat mesangial cells, *Exp. Clin. Endocrinol. Diabetes* 127 (2019) 630–640.
- [51] L.C. Ho, J.M. Sung, Y.T. Shen, H.F. Jheng, S.H. Chen, P.J. Tsai, Y.S. Tsai, Egr-1 deficiency protects from renal inflammation and fibrosis, *J. Mol. Med. (Berl.)* 94 (2016) 933–942.
- [52] K. Inoue, G. Gan, M. Ciarleglio, Y. Zhang, X. Tian, C.E. Pedigo, C. Cavanaugh, J. Tate, Y. Wang, E. Cross, M. Groener, N. Chai, Z. Wang, A. Justice, Z. Zhang, C. R. Parikh, F.P. Wilson, S. Ishibe, Podocyte histone deacetylase activity regulates murine and human glomerular diseases, *J. Clin. Invest.* 129 (2019) 1295–1313.
- [53] D. Wang, M.P. Guan, Z.J. Zheng, W.Q. Li, F.P. Lyv, R.Y. Pang, Y.M. Xue, Transcription factor Egr1 is involved in high glucose-induced proliferation and fibrosis in rat glomerular mesangial cells, *Cell. Physiol. Biochem.* 36 (2015) 2093–2107.
- [54] E.P. Brennan, M. Mohan, A. McClelland, C. Tikellis, M. Ziemann, A. Kaspi, S. P. Gray, R. Pickering, S.M. Tan, S.T. Ali-Shah, P.J. Guiry, A. El-Osta, K. Jandeleit-Dahm, M.E. Cooper, C. Godson, P. Kantharidis, Lipoxins regulate the early growth response-1 network and reverse diabetic kidney disease, *J. Am. Soc. Nephrol.* 29 (2018) 1437–1448.